Article

Neuron

Satb1 Regulates Contactin 5 to Pattern Dendrites of a Mammalian Retinal Ganglion Cell

Highlights

- Satb1 is expressed by ON-OFF direction-selective retinal ganglion cells (ooDSGCs)
- Satb1 is required for the characteristic bistratification of ooDSGC dendrites
- Effects of Satb1 are mediated in part by the homophilic adhesion molecule Contactin 5
- Contactin 5-mediated homophilic binding to interneurons stabilizes ooDSGC dendrites

Authors

Yi-Rong Peng, Nicholas M. Tran, Arjun Krishnaswamy, Dimitar Kostadinov, Emily M. Martersteck, Joshua R. Sanes

Correspondence

sanesj@mcb.harvard.edu

In Brief

Peng et al. show that the transcription factor Satb1 is selectively expressed in a subset of retinal ganglion cells and controls the shape of their dendritic arbor by regulating Contactin 5, which mediates branch-specific homophilic adhesion to interneurons.

Peng et al., 2017, Neuron *95*, 869–883
August 16, 2017
http://dx.doi.org/10.1016/j.neuron.2017.07.019

CellPress

Neuron
Article

Satb1 Regulates Contactin 5 to Pattern Dendrites of a Mammalian Retinal Ganglion Cell

Yi-Rong Peng,[1] Nicholas M. Tran,[1] Arjun Krishnaswamy,[1,2] Dimitar Kostadinov,[1,3] Emily M. Martersteck,[1] and Joshua R. Sanes[1,4,*]
[1]Center for Brain Science and Department of Molecular and Cellular Biology, Harvard University, Cambridge, MA, USA
[2]Present address: Department of Physiology, McGill University, Montreal, QC, Canada
[3]Present address: Department of Neuroscience, Physiology and Pharmacology, University College London, London, UK
[4]Lead Contact
*Correspondence: sanesj@mcb.harvard.edu
http://dx.doi.org/10.1016/j.neuron.2017.07.019

SUMMARY

The size and shape of dendritic arbors are prime determinants of neuronal connectivity and function. We asked how ON-OFF direction-selective ganglion cells (ooDSGCs) in mouse retina acquire their bistratified dendrites, in which responses to light onset and light offset are segregated to distinct strata. We found that the transcriptional regulator Satb1 is selectively expressed by ooDSGCs. In *Satb1* mutant mice, ooDSGC dendrites lack ON arbors, and the cells selectively lose ON responses. Satb1 regulates expression of a homophilic adhesion molecule, Contactin 5 (*Cntn5*). Both Cntn5 and its co-receptor Caspr4 are expressed not only by ooDSGCs, but also by interneurons that form a scaffold on which ooDSGC ON dendrites fasciculate. Removing Cntn5 from either ooDSGCs or interneurons partially phenocopies *Satb1* mutants, demonstrating that Satb1-dependent *Cntn5* expression in ooDSGCs leads to branch-specific homophilic interactions with interneurons. Thus, Satb1 directs formation of a morphologically and functionally specialized compartment within a complex dendritic arbor.

INTRODUCTION

Among the features by which we distinguish classes of neurons from each other, dendritic morphology ranks high. This was a main criterion used by Ramón y Cajal in the nineteenth century (Ramón y Cajal, 1909), and it remains a powerful criterion today. Many neurobiologists can identify cerebellar Purkinje cells, cortical pyramid neurons, or spinal motor neurons based on dendritic shape alone. Importantly, dendritic arbors are not mere plumage: their size, shape, and location are critical determinants of the numbers and types of inputs that each neuron receives (Lefebvre et al., 2015; London and Häusser, 2005).

Substantial distinctions also occur among neuronal types within a general class. Here, retinal ganglion cells (RGCs) provide a good example. RGCs in the ganglion cell layer all send one or a few primary dendrites into the inner plexiform layer (IPL), where they branch to form planar arbors confined to narrow strata. Yet, arbors of individual RGC types, of which there are >30 in mice, differ in multiple ways, including symmetry, diameter, branch density, and stratification level (Sanes and Masland, 2015) (Figure 1A). Their diameter and shape are directly related to the size and shape of their receptive field, respectively. Their stratification level is a prime determinant of the interneuron types from which they receive synapses and, therefore, the visual features to which they respond. Thus, RGCs provide a useful system for exploring how neurons within a class acquire type-specific dendritic features.

Studies in multiple systems have revealed three sets of factors that control dendritic morphogenesis: intrinsic transcriptional programs, signals from neighboring cells, and (at least for vertebrates) activity-dependent remodeling (Dong et al., 2015; Lefebvre et al., 2015). Studies of the dendritic arborization (da) neurons in *Drosophila* provide an influential model for transcriptional control of type-specific arborization patterns. Four groups of da neurons (called I–IV) elaborate dendrites that innervate the body wall. They differ, however, in dendritic complexity (I least, IV most). The four groups are distinguished by differential expression of a set of conserved transcription factors that determine class-specific arborization patterns by regulating expression of cytoskeletal and adhesive molecules (Corty et al., 2009; Grueber et al., 2003; Jinushi-Nakao et al., 2007; Kim et al., 2006; Li et al., 2004; Sugimura et al., 2004). The adhesion molecules, in turn, interact with environmental cues, leading to appropriate patterns of dendritic growth and arborization (Parrish et al., 2007; Santiago and Bashaw, 2014). It is likely that this logic is evolutionally conserved (Cubelos et al., 2010; Peng et al., 2009; Puram and Bonni, 2013; Valnegri et al., 2015; Whitney et al., 2014), but in few, if any, cases have genetic programs been identified that control individual features within complex dendrites.

Here, we analyzed RGCs to address this issue, focusing on a particularly well-studied type, the ON-OFF direction-selective RGCs (ooDSGCs) (Vaney et al., 2012). ooDSGCs have bistratified dendritic arbors. Inputs sensitive to increased and decreased illumination levels are confined to the inner (ON) and outer (OFF) strata of the IPL, respectively, thus accounting for their dual responsiveness. There are four ooDSGC types, each responsive to motion in one of four directions (ventral, dorsal, nasal, and temporal) (Oyster and Barlow, 1967). The four

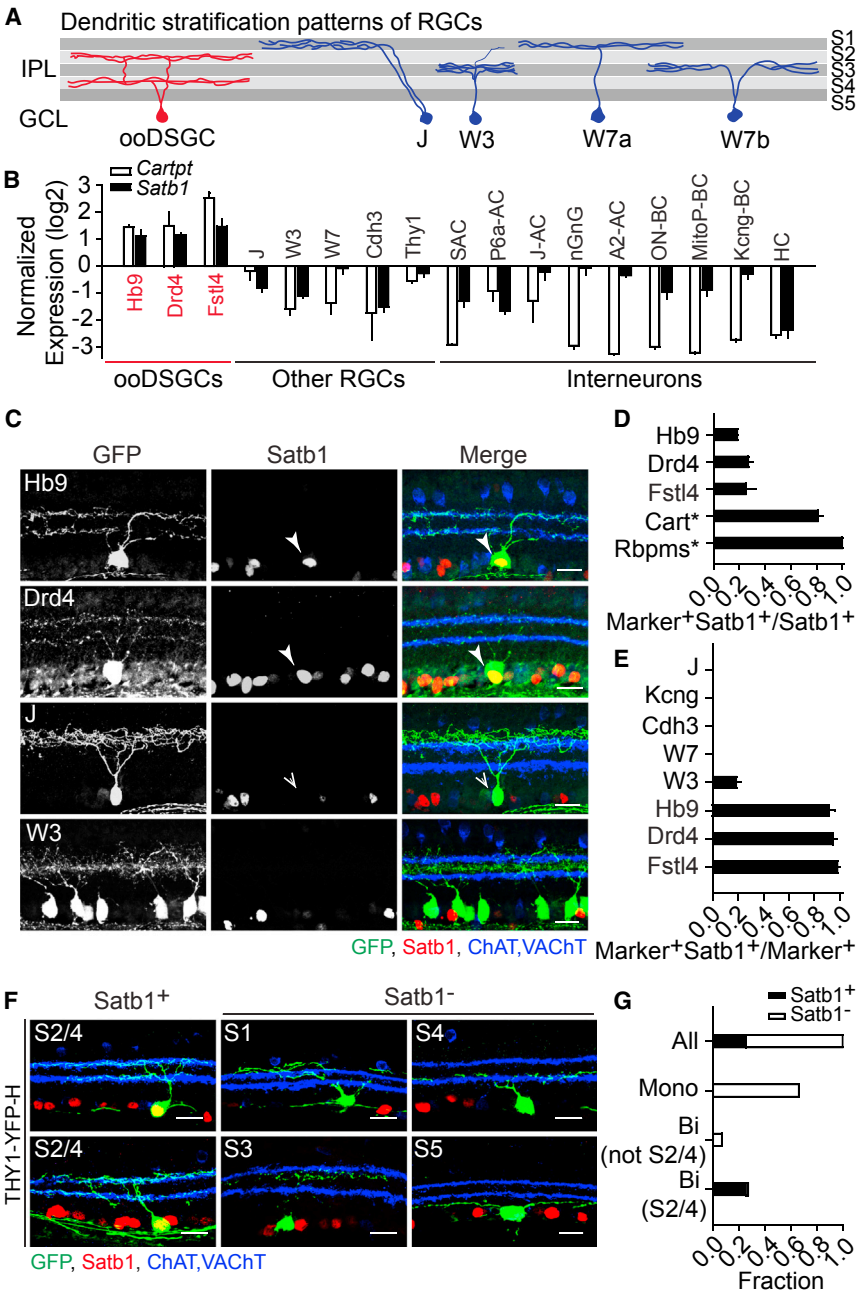

Figure 1. ooDSGCs Selectively Express *Satb1*

(A) Sketch of bistratified ooDSGCs and selected monostratified RGC types. IPL, inner plexiform layer; S1-5, IPL sublaminae; GCL, ganglion cell layer.

(B) Microarray analysis of *Satb1* and *Cartpt* expression in retinal cells isolated by FACS from transgenic lines. Expression values were log2 transformed and centered on their mean values across all the samples. *Cartpt* was previously shown to be selectively expressed by ooDSGCs and a set of amacrine cells. Transgenic lines are described in STAR Methods and Kay et al. (2012). AC, amacrine cells; BC, bipolar cells; HC, horizontal cells.

(C) Immunostaining of Satb1 (red in merge) in sections from transgenic lines that label ooDSGCs (Hb9-GFP and Drd4-GFP) or other RGCs (J-RGCs in JamB-CreER and W3-RGCs in TYW3) at P14. S2 and S4 laminae are marked with anti-ChAT and anti-VAChT (blue in merge). Arrowheads indicate Satb1-positive cells; open arrowhead indicates a Satb1-negative cell.

(D) Fraction (±SEM) of Satb1-positive cells that are also transgene positive in Hb9-GFP, Drd4-GFP, and Fstl4-CreER, each of which labels one of four ooDSGC types, or those that are labeled by anti-Cart or anti-Rbpms. Asterisk indicates cells labeled by antibodies. ≥3 P14–P21 animals per line, >20 cells per animal.

(E) Fraction (±SEM) of transgene-positive RGCs that are Satb1 positive in indicated lines. ≥3 P14–P21 animals per line, >20 cells per animal.

(F) Immunostaining of Satb1 in retinas from P21 Thy1-YFPH mice. Micrographs show two bistratified RGCs (S2/4) that are Satb1 positive and four monostratified RGCs (S1, S3, S4, and S5) that are Satb1 negative.

(G) Fraction of Thy1-YFPH-marked RGCs that were Satb1 positive or negative. RGCs were divided into monostratified (Mono), bistratified (Bi, not S2/4), and bistratified (Bi, S2/4 = ooDSGC) populations. 25% of YFP-positive RGCs were bistratified cells, 94% of which were Satb1 positive. 3 animals, 59 cells.

Scale bars represent 20 μm.

types share many structural and physiological properties but exhibit some molecular differences (Huberman et al., 2009; Kay et al., 2011a; Morrie and Feller, 2016). To find genes involved in establishing type-specific features, we used a gene expression database generated from 17 sets of retinal cells that we had transcriptionally profiled (Kay et al., 2011b, 2012). To improve our chance of finding genes involved in ooDSGC dendritic morphogenesis, we sought transcriptional regulators that were expressed by two ooDSGC types with different directional preferences but not by other RGCs. Satb1 (special AT-rich sequence-binding protein 1), recently implicated in development of cortical interneurons (Close et al., 2012; Denaxa et al., 2012), fulfilled this criterion. We showed that Satb1 acts cell autonomously in ooDSGCs to generate bistratified arbors; in its absence, ooDSGCs selectively lose their ON arbor and become unresponsive to light-on stimuli. We then compared transcriptome profiles of control and *Satb1*$^{-/-}$ ooDSGCs to seek cell surface proteins that could act downstream of Satb1 and mediate its morphogenetic effects. We found that the immunoglobulin superfamily member Contactin 5 (Cntn5) is one such molecule: its expression is regulated by Satb1, and its deletion leads to dendritic alterations similar to those of *Satb1* deletion. Finally, we present evidence that Cntn5 and its co-receptor Caspr4 may act by mediating homophilic adhesion to Cntn5/Casp4-expressing interneurons that form a scaffold for the ooDSGC ON arbor. Together, our results elucidate a genetic

pathway that generates type-specific features in the dendrites of RGCs.

RESULTS

Satb1 Is Selectively Expressed in ooDSGCs

To seek transcriptional regulators selectively expressed by ooDSGCs, we used a gene expression database obtained by transcriptomic profiling of 17 sets of retinal neurons isolated by FACS from transgenic mouse lines (Kay et al., 2011b, 2012; J.N. Kay, Y.-R.P., and J.R.S., unpublished data). It included eight groups of RGCs, five groups of amacrine cells, three groups of bipolar cells, and horizontal cells. Of the RGCs, three were ooDSGCs: Hb9-GFP and Fstl4-CreER;stop-YFP lines label ooDSGCs that prefer ventral motion on the retina (V-ooDSGCs) (Kim et al., 2010; Trenholm et al., 2011); and the Drd4-GFP line labels nasal-preferring ooDSGCs (N-ooDSGCs) (Huberman et al., 2009; Kay et al., 2011a). We compared expression profiles to that of *Cartpt*, which encodes Cart, a peptide that is present in most, if not all, ooDSGCs (Kay et al., 2011a). *Satb1*, like *Cartpt*, was expressed at higher levels in all three ooDSGC populations than in any other retinal type represented in the database (Figure 1B).

To validate the expression of Satb1 in ooDSGCs, we stained retinas with anti-Satb1 (Figure 1C). Satb1 was present in a subset of RGCs, identified by the pan-RGC marker Rbpms (Rodriguez et al., 2014), but not in any other retinal cells, including photoreceptors, interneurons, or Müller glia (Figure 1D; Figure S1A). 80% of Satb1-positive RGCs were Cart positive, and the three ooDSGC-specific lines (Hb9-GFP, Drd4-GFP, and Fstl4-CreER; stop-YFP) each labeled ~20% of Satb1-positive cells, consistent with the fact that each line marks one of the four ooDSGCs types (Figure 1D) (Kay et al., 2011b). Moreover, >90% of ooDSGCs labeled in each of these lines were Satb1 positive (Figure 1E). In contrast, no RGCs were detectably Satb1 positive in several lines that label monostratified RGCs or bistratified RGCs that arborize in laminae distinct from those in which ooDSGCs arborize (Figure 1E) (Duan et al., 2015; Kim et al., 2008; Osterhout et al., 2011). Thus, most Satb1-positive retinal cells are ooDSGCs. The remaining Satb1-positive cells include a small fraction of RGCs labeled in the TYW3 line (Kim et al., 2010; Krishnaswamy et al., 2015), some of which are Foxp2 positive (Rousso et al., 2016); most of these contain lower levels of Satb1 than do ooDSGCs.

In a complementary approach, we used the Thy1-YFPH line, which labels ~200 RGCs per retina (Feng et al., 2000). Labeling is sufficiently sparse in this line to assess cellular morphology, and previous studies showed that most RGC types are represented (Coombs et al., 2006; Samuel et al., 2011). Over 90% of the YFP, Satb1 double-positive RGCs were bistratified with arbors in S2 and S4 (we divide the IPL into five equal strata, with S1 neighboring the inner nuclear layer and S5 neighboring the ganglion cell layer; see Figure 1A) (Figures 1F and 1G). Together, these results demonstrate that nearly all retinal cells brightly stained for Satb1 are ooDSGCs.

Satb1 Is Required for Patterning ooDSGCs Dendritic Arbors

To assess the function of Satb1 in ooDSGCs, we crossed a null allele (Close et al., 2012) to the Hb9-GFP and Drd4-GFP lines, which mark V-ooDSGCs and N-ooDSGCs, respectively. Results were similar in both lines. We discuss V-ooDSGCs here and return to subtle, but informative, differences between V- and N-ooDSGCs below. Retinal structure was not detectably perturbed in the absence of Satb1 (Figure S1). However, whereas dendrites of wild-type ooDSGCs are bistratified with arbors in S2 and S4, mutant ooDSGC dendrites were monostratified, retaining their outer arbor in S2 but lacking their inner arbor in S4 (Figures 2A and 2B).

We assessed the specificity of this phenotype in two ways. First, we examined lamina-specific arborization of ten other groups of retinal neurons. In no case did lamination differ detectably between Satb1 mutants and controls (Figure S1). Second, we asked whether other properties of ooDSGCs were regulated by Satb1. Loss of Satb1 had no detectable effects on the number or spacing of ooDSGCs or on their projections to targets in the brain (Figure S2). Moreover, ooDSGCs in *Satb1*$^{-/-}$ retina neither lost their characteristic markers nor acquired markers of other RGC types (Figure S3). Thus, Satb1 acts selectively on dendritic morphogenesis without causing a more global fate change.

To evaluate dendritic morphology quantitatively, we traced and measured individual ooDSGC arbors from sparsely labeled regions in whole mounts; these were generally in peripheral retina. Consistent with results from sections, S2 (OFF) and S4 (ON) arbors were similar in size in controls, but ON arbors were far smaller than OFF arbors in mutants (Figure 2C). Moreover, whereas S4 branches are planar in controls, those that persisted in S4 of mutants were generally ascending toward S2 (Figures 2D and 2E). Despite loss of the ON arbor, the total dendritic length and the total number of branch points did not differ significantly between mutants and controls (Figures 2F and 2G). Instead, the decrease in dendritic arbor branching in S4 was compensated by an increased branch density in S2, leading to a slight broadening of the S2 arbor (Figures 2B, 2D, 2E, and 2H–2J). Thus, Satb1 does not control the overall elaboration of dendritic branches in ooDSGCs, but rather their position: branches divided between S2 and S4 in controls are directed to S2 in mutants.

Satb1 Acts to Stabilize the ooDSGC ON Arbor

We next analyzed the formation of ooDSGC arbors during early postnatal life. Previous work showed that dendrites of ooDSGCs are largely restricted to S2 and S4 by postnatal days 5 and 6 (P5 and P6) (Kim et al., 2010). Analysis at earlier stages revealed that ooDSGC arbors were concentrated in a broad band in the inner portion of the IPL at P3, before becoming bistratified (Figures 3A–3C). Arbors in *Satb1* mutants and controls were similar until P6: branches first extended in S4 and then formed a second plexus in S2. In controls, however, arbors remained bistratified, whereas in mutants, the nascent S4 arbor was lost after P6, leading to a monostratified arbor centered in S2 (Figures 3A and 3D–3F). Together, these results define three stages in the development of ooDSGC arbors: formation of a broad S4 arbor between birth and P3; splitting into distinct S2 and S4 arbors between P3 and P6; and growth and stabilization of the arbors between P6 and P9. In Satb1

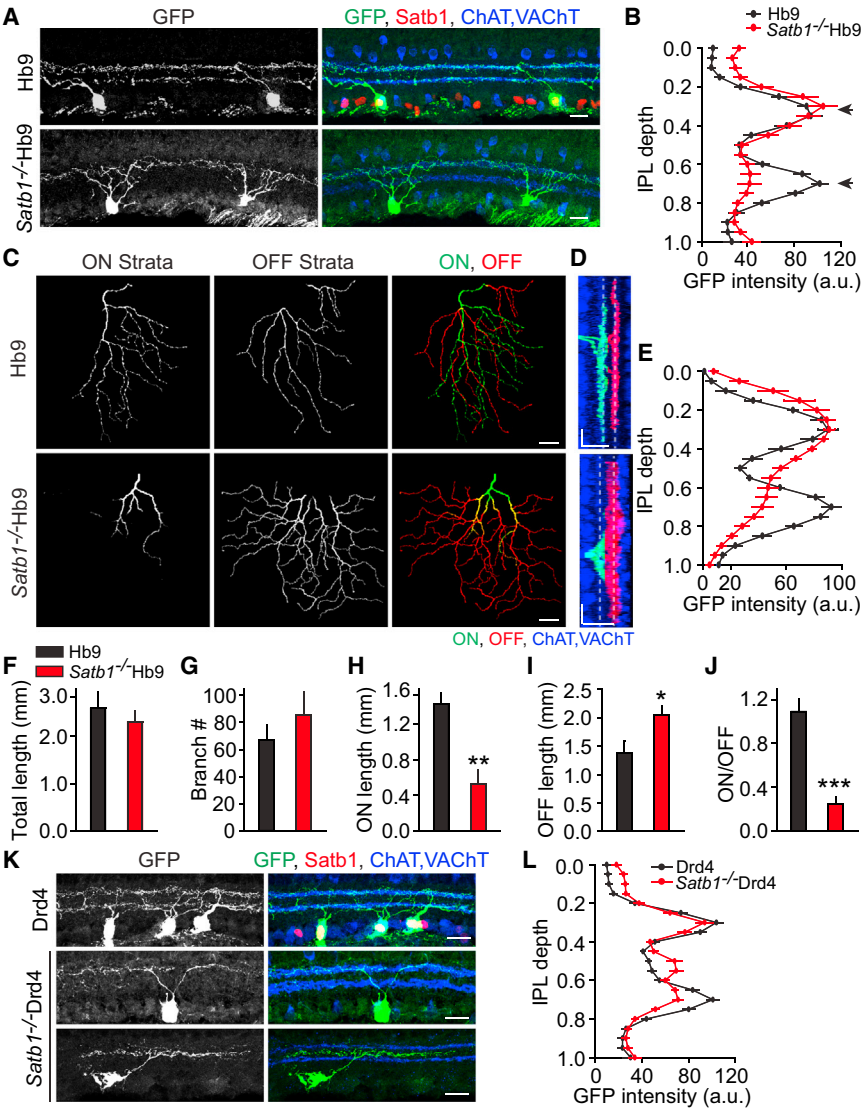

Figure 2. ooDSGCs Dendrites Are Monostratified in the Absence of Satb1

(A) Hb9-GFP RGCs from P14 wild-type and *Satb1*$^{-/-}$ retinas stained as in Figure 1C.

(B) Mean intensity (±SEM) of GFP-labeled dendritic processes across the IPL from sections such as those in (A) (n = 11, wild-type; 13, *Satb1*$^{-/-}$). 0 and 1 are borders of inner nuclear layer and ganglion cells layer, respectively. Peaks of ChAT + VAChT staining from Figure S1 are shown as arrows.

(C) Dendrites of Hb9-GFP RGCs reconstructed from whole mounts of P14 wild-type and *Satb1*$^{-/-}$ retinas. ON and OFF strata, determined by ChAT + VAChT staining, are shown in green and red, respectively.

(D) Rotation of cells in (C) to show the stratification. S2 and S4 laminas, marked by anti-ChAT and VAChT, are indicated by white dashed lines.

(E) Mean intensity (±SEM) of GFP-labeled dendritic processes across the IPL from images such as those in (D) (n = 5 for each genotype).

(F–J) Wild-type and mutant Hb9-GFP dendrites do not differ in total dendritic length (F) or branch point number (G), but ON arbors are smaller (H) and OFF arbors are larger (I) in mutants than wild-types. The ON/OFF ratio of arbor length is decreased in *Satb1*$^{-/-}$;Hb9 (J). Measurements are from data in (C). Error bars represent SEM. ***p < 0.001, **p < 0.01, *p < 0.05 by t test.

(K) Drd4-GFP RGCs from P16 wild-type and *Satb1*$^{-/-}$ retinas stained as in Figure 1C.

(L) Mean intensity (±SEM) of GFP-labeled dendritic processes across the IPL from sections such as those in (K) (n = 14, control; 33, mutant).

See also Figures S1–S4. Scale bars represent 20 μm.

mutants, the first two stages proceed normally, but the S4 arbor is not maintained (Figure 3G).

Satb1 Patterns ooDSGC Dendrites Postnatally and Cell Autonomously

Although the *Satb1* mutant phenotype is apparent after P6, the defects could result from an earlier requirement for Satb1 in the ooDSGC developmental program. To test this possibility, we used conditional *Satb1* mutants (*Satb1*$^{fl/fl}$) to delete *Satb1* from ooDSGCs postnatally a week after they become postmitotic (De la Huerta et al., 2012). We generated *Satb1*$^{fl/fl}$;Hb9-GFP mice and used adeno-associated viral (AAV) vectors to introduce cre at P0, deleting *Satb1* from only some ooDSGCs; mutant and control cells were distinguished by staining with anti-Satb1. When examined at P14, ooDSGCs from which *Satb1* had been deleted bore monostratified dendrites, whereas nearby cells that retained Satb1 had bistratified dendrites (Figures 3H and 3I). In contrast, infection at P3 had no detectable effects on dendritic stratification. We draw three conclusions from these results: First, Satb1 acts late in the developmental program that patterns ooDSGC dendritic arbors. Second, its requirement is confined to a restricted postnatal period. Finally, it acts cell autonomously.

Satb1 Is Required for ON Responses of ooDSGCs

As noted above, inputs that convey information about ON stimuli (typically bright stationary or moving objects on a dark background) and OFF stimuli (dark objects on a bright background) are segregated on ooDSGC dendritic arbors: ON- and OFF-responsive excitatory and inhibitory interneurons synapse selectively on S4 and S2 arbors, respectively (Vaney et al., 2012). In *Satb1*$^{-/-}$ mice, S4 (ON) dendrites may be translocated to S2, the OFF sublamina. They might carry their inputs with them, remain uninnervated, or receive OFF inputs. To distinguish these and other possibilities, we targeted control and mutant GFP-positive ooDSGCs in the Hb9-GFP line for loose-patch recording. Because constitutive *Satb1* mutants die shortly after weaning (~P21), we used conditional mutants for these studies and induced retina-specific deletion with a transgenic line (Furuta et al., 2000).

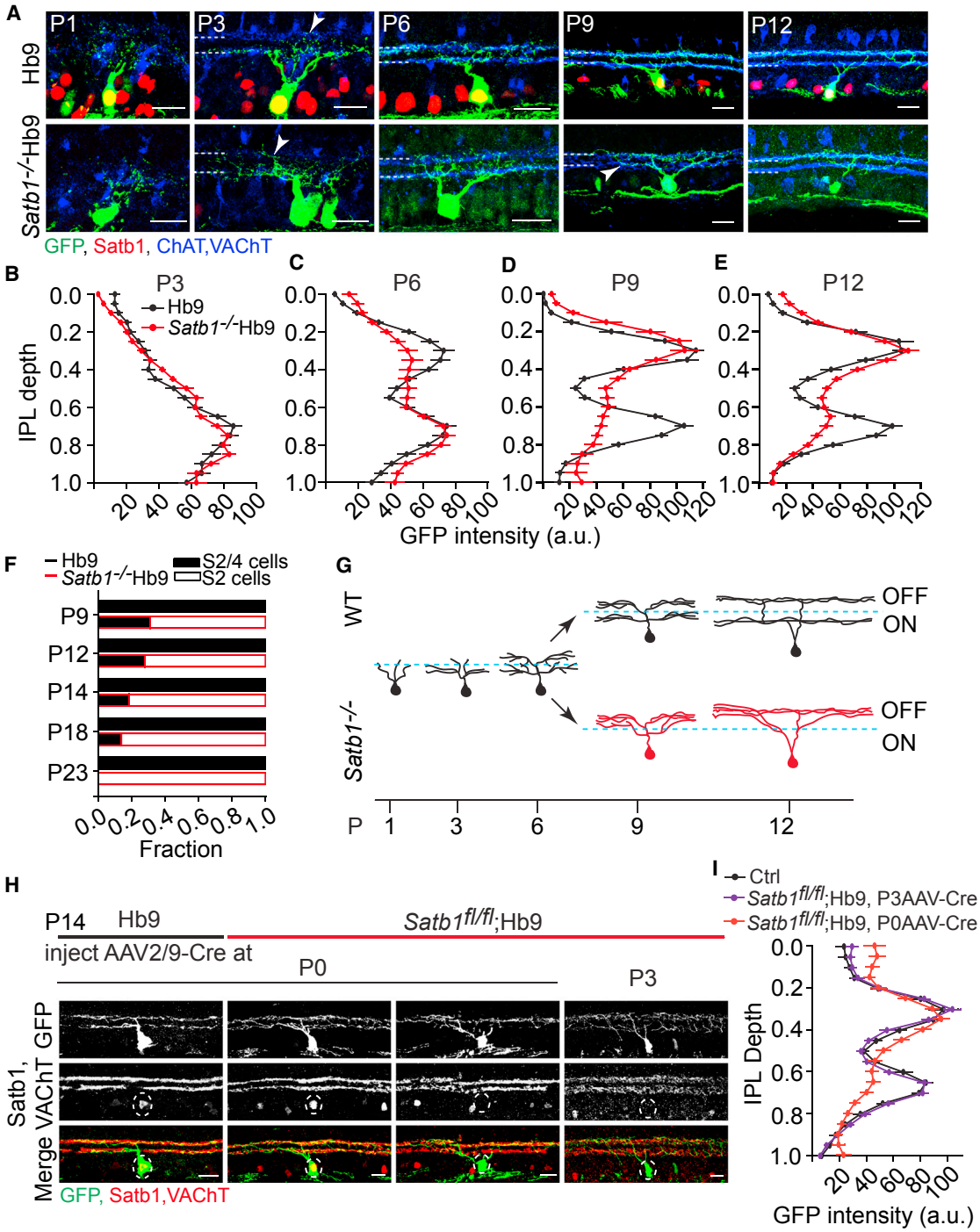

Figure 3. Satb1 Acts on ooDSGCs Postnatally and Cell Autonomously

(A) Retinal sections from Hb9-GFP and *Satb1*$^{-/-}$;Hb9-GFP mice at indicated ages, stained as in Figure 1C. Arrowheads indicate dendrites sprouting into S2 at P3 and ascending dendrites from S4. S2 and S4 are highlighted by white dashed lines.

(B–E) Mean intensity (±SEM) of GFP-labeled dendritic processes across the IPL from sections such as those in (A) at P3 (B), P6 (C), P9 (D), and P12 (E). n = 10–21 (mean = 16) per genotype per age.

(F) Fraction of S2/4 bistratified and S2 monostratified Hb9-GFP RGCs from control and *Satb1*$^{-/-}$ retinas at indicated ages. n = 11–59 RGCs (mean 28) per genotype per age.

(G) Sketch illustrating dendritic morphogenesis of control and *Satb1*$^{-/-}$;Hb9-GFP ooDSGCs. Blue dashed line marks the separation between ON and OFF portions of IPL.

(legend continued on next page)

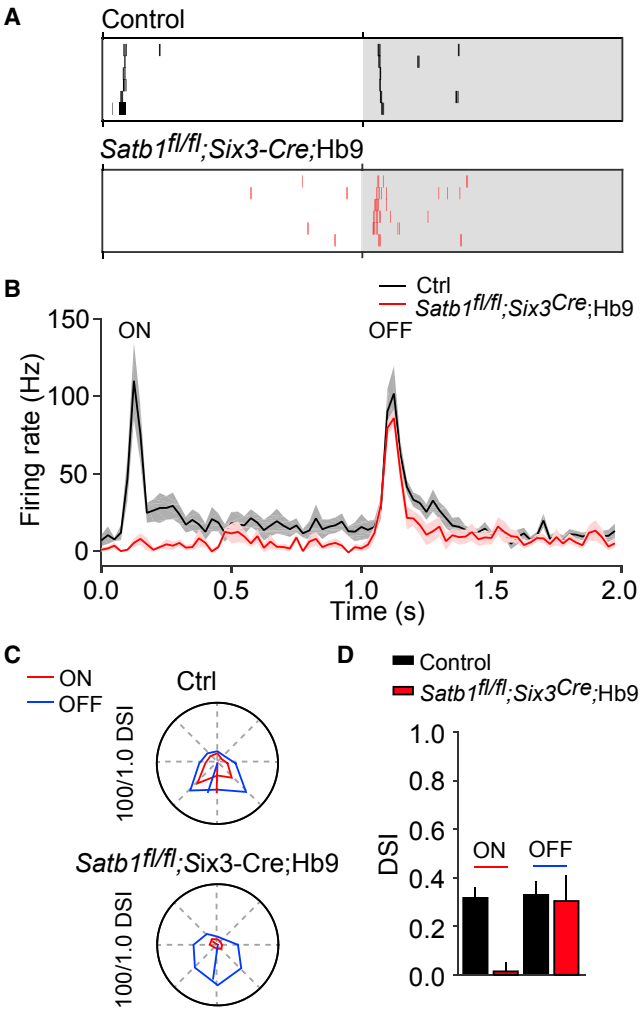

Figure 4. ON Responses of ooDSGCs Are Lost in the Absence of Satb1

(A) Spike raster plots from Hb9-GFP RGCs in control and *Satb1* mutant retinae in response to an ~200 μm flashing spot centered on the receptive field (six trials). Mutant ooDSGCs lack ON responses.

(B) Average firing rates of Hb9-GFP (n = 10) and Satb1 mutant Hb9-GFP RGCs (n = 6) in response to stimulation as in (A). Solid lines indicate average values. Shadowing denotes SEM. Bin width, 25 ms.

(C) Polar plots for firing rates (octagons) and direction selectivity index (DSI; lines) from control and Satb1 mutant Hb9-GFP RGC in response to a bright bar moving in eight different directions. Radius = 100 Hz, 1.0 DSI.

(D) Average DSI from control (n = 10) and mutant (n = 6) Hb9-GFP RGCs computed from population vectors such as those in (C).

We first stimulated ooDSGCs with spots of light (~200 μm in diameter, 1 s duration). As expected, control ooDSGCs responded vigorously to both the onset (ON response) and offset (OFF response) of the stimulus. In contrast, mutant ooDSGCs retained normal OFF responses but lacked ON responses (Figures 4A and 4B). Thus, excitatory inputs from ON bipolar cells are unlikely to form functional synapses on ooDSGC dendrites that might translocate to the OFF sublamina. As an additional test, we stained axonal arbors of type 5 bipolars, which deliver ON input to S4 (Duan et al., 2014) with anti-CaBP5; their position was not detectably affected in *Satb1* mutant retina (Figure S1D).

To assess inhibitory responses, we made use of the fact that the direction selectivity of ooDSGCs is patterned by inhibition from starburst amacrine cells (SACs) (Fried et al., 2002; Wei et al., 2011). The direction selectivity of the OFF response did not differ detectably between *Satb1*$^{-/-}$ and control ooDSGCs, indicating that inhibitory inputs to the OFF arbor were normal (Figures 4C and 4D). Thus, Satb1 is required for ON responses of ooDSGCs but dispensable for responsiveness and direction selectivity within the OFF channel.

Satb1 Differentially Affects Dendrites of V-ooDSGCs and N-ooDSGCs

Analysis of *Satb1* mutants described to this point was performed on V-ooDSGCs labeled in the Hb9-GFP line. We used two additional lines to analyze other ooDSGC populations: Drd4-GFP, which marks nasal motion-preferring N-ooDSGCs, and *Cartpt*^{Cre}, which, like CART staining, marks all ooDSGCs as well as some amacrine cells. *Satb1* deletion had a similar effect on all classes of ooDSGCs: the normally bistratified dendritic arbor became monostratified in the absence of *Satb1* (Figures 2K and 2L; Figures S4A and S4B). We analyzed N-ooDSGCs further. For N-ooDSGCs as for V-ooDSGCs, the defect reflected instability of the ON arbor (Figure S4C). However, further analysis revealed a difference between phenotypes in N-ooDSGCs and V-ooDSGCs. Approximately one-third of mutant N-ooDSGCs resembled mutant V-ooDSGCs in that they retained only the S2 arbor. Another third were also monostratified, but their arbor was centered on S3. The final third retained a bistratified dendritic morphology (Figures S4D and S4E).

What accounts for the difference in Satb1's role between V-ooDSGCs and N-ooDSGCs? We considered the possibility that these two RGC types might differentially express *Satb2*, a homolog of *Satb1*. *Satb2* was expressed by both V-ooDSGCs and N-ooDSGCs at P14 (Figure S4F), as well as in subsets of other RGCs and amacrine cells (Kay et al., 2011b). At P1 and P3, however, *Satb2* was expressed in significantly more N-ooDSGCs than V-ooDSGCs (Figures S4G and S4H). Moreover, in *Satb1*$^{-/-}$ retina, Satb2 was lost from most V-ooDSGCs but retained by ~70% of N-ooDSGCs (Figure S4H). Thus, we speculate that Satb2, as well as Satb1, controls ooDSGCs dendritic arborization, but that key differences in their regulation affect their relative contribution in V-ooDSGCs and N-ooDSGCs.

Satb1 Regulates Cntn5 Expression in ooDSGCs

Satb1 presumably acts in ooDSGCs by directly or indirectly regulating expression of genes involved in dendritic growth, stability, or patterning. To seek such genes, we isolated ooDSGCs

(H) Retinal sections from P14 Hb9-GFP and Satb1$^{fl/fl}$;Hb9-GFP mice following injection with AAV-cre at P0 or P3. *Satb1* deletion at P0, but not P3, leads to stratification changes. ooDSGC somata are outlined by dashed circles. Anti-Satb1 and VAChT are red in merge.

(I) Mean intensity (±SEM) of GFP-labeled dendritic processes across the IPL from sections such as those in (H) (n = 10, control; 16, either Satb1$^{fl/fl}$;Hb9 condition). See also Figure S4. Scale bars represent 20 μm.

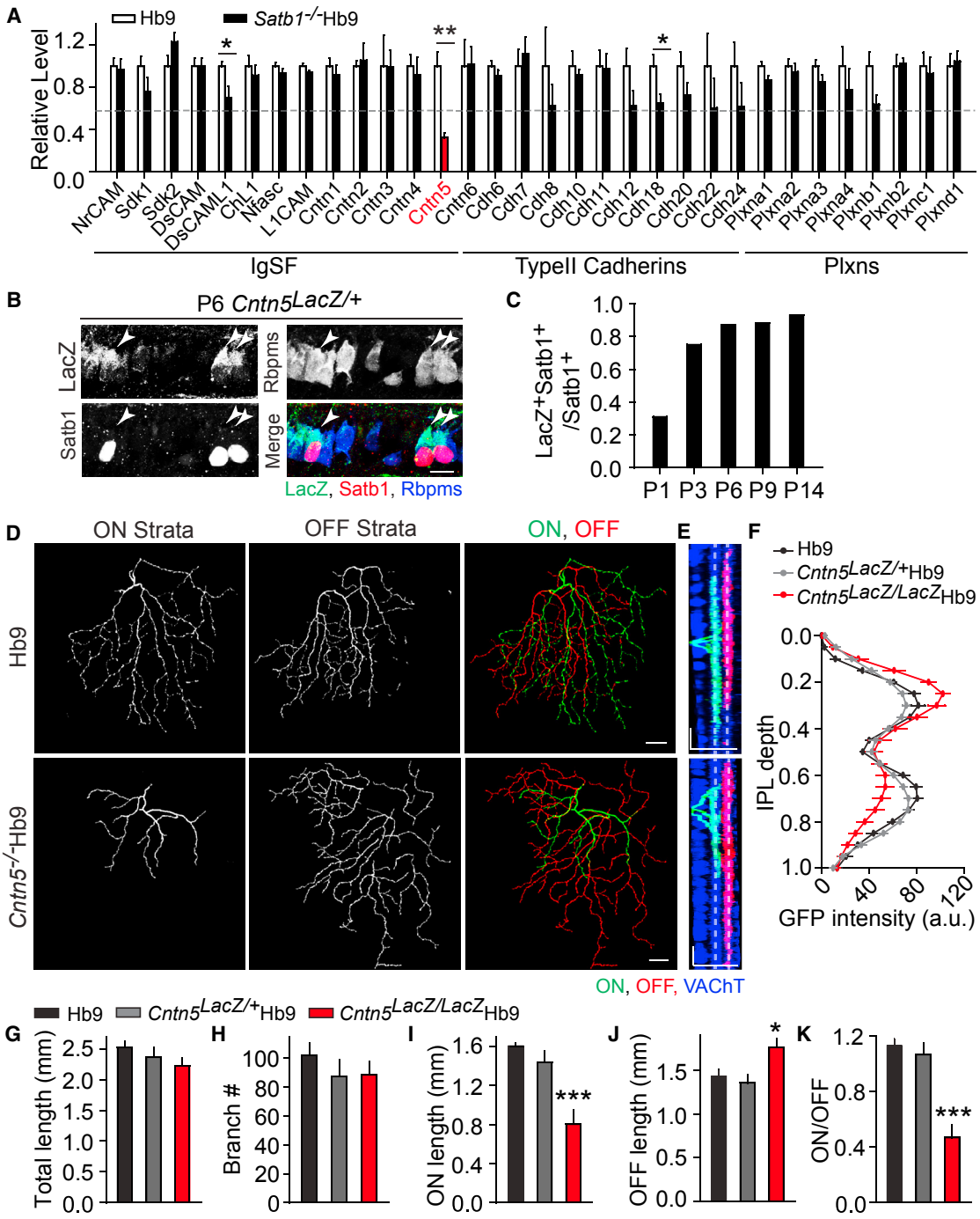

Figure 5. *Cntn5* Is Regulated by Satb1 and Required for ooDSGC Arbor Formation

(A) Expression levels of immunoglobulin superfamily members (IgSF), type II cadherins, and plexins (Plxns) in *Satb1*$^{-/-}$;Hb9-GFP RGCs compared to those in control Hb9-GFP RGCs as determined by RNA-seq.

(B) Section of P6 *Cntn5*$^{LacZ/+}$ retina stained for anti-LacZ (green in merge), Satb1 (red in merge), and Rbpms (blue in merge). Arrowheads indicate Satb1-positive RGCs.

(C) Fraction of Satb1-positive RGCs that are LacZ positive in *Cntn5*$^{LacZ/+}$ retinas at indicated ages; n > 40, 2 animals per age.

(D) Dendrites of single Hb9-GFP RGCs reconstructed from whole mounts of P21 wild-type and *Cntn5*$^{LacZ/LacZ}$ retina. ON and OFF strata are shown in green and red, respectively.

(E) Rotation of stacks in (D). S2 and S4 laminas, marked by anti-ChAT and VAChT staining (blue), are highlighted by white dashed lines.

(legend continued on next page)

by fluorescence-activated cell sorting (FACS) from Hb9-GFP and *Satb1*$^{-/-}$;Hb9-GFP mice and analyzed their transcriptomes by RNA sequencing (RNA-seq). Approximately 95 genes were significantly regulated by Satb1 ($p < 0.01$), 19 being upregulated and 76 being downregulated, in mutants compared to controls (Table S1).

We focused on transmembrane recognition molecules, such as immunoglobulin superfamily molecules, cadherins, and plexins, which have been implicated in synaptic choices of retinal interneurons and RGCs (Duan et al., 2014; Krishnaswamy et al., 2015; Sun et al., 2013; Yamagata and Sanes, 2008). Among genes surveyed, the immunoglobulin superfamily member Cntn5 showed the most striking reduction in the *Satb1*$^{-/-}$; Hb9-GFP cells (Figure 5A). qPCR performed on independently isolated sets of control and mutant V-ooDSGCs confirmed the reduction (Figure S5A).

For further analysis, we used the *Cntn5*^{LacZ} mouse line, in which a tau-beta galactosidase (LacZ) fusion was inserted into the *Cntn5* locus (Li et al., 2003). We showed recently that a set of ON bipolars express Cntn5 in mature retina (Shekhar et al., 2016). In young retina, however, the majority of LacZ-positive cells were ooDSGCs (Figure 5B; Figure S5B). Expression appeared during the first several postnatal days, and 80% of ooDSGCs were LacZ positive by P6 (Figure 5C). *Cntn5* expression in bipolar cells was detectable after P8 (Figure S5E).

Contactin 5 and Satb1 Mutants Have Similar Effects on ooDSGC Dendritic Arbors

We next used the *Cntn5*^{LacZ} line, which is a null allele, to ask whether Cntn5 plays a role in patterning ooDSGC dendrites. Dendritic defects in *Cntn5*$^{LacZ/LacZ}$ mice were qualitatively similar to those described above for *Satb1* mutants: S4 (ON) arbors of V-ooDSGCs were disrupted in *Cntn5*$^{LacZ/LacZ}$ mice, but S2 (OFF) arbors persisted (Figures 5D–5F; Figures S5C and S5D), and the S2 arbor was enhanced to the same extent that the S4 arbor was diminished (Figures 5G–5K). The phenotype was selective in that retinal organization was not detectably perturbed in the absence of *Cntn5*, and lamina-specific arbors were not disrupted in other cell types assayed (Figures S5E–S5G). For each parameter measured, however, effects were quantitatively less severe in *Cntn5* $^{LacZ/LacZ}$ mice than in *Satb1*$^{-/-}$ mice. These results indicate that the effects of Satb1 on ooDSGC morphogenesis are mediated in part, but not entirely, by Cntn5.

Contactin5 Is Expressed by ON, but Not OFF, Starburst Amacrine Cells

Cntn5 could interact with ligands on neighboring cells to stabilize the ON arbor. What might those cells be? SACs are attractive candidates. ooDSGC dendrites fasciculate on SAC dendrites, from which they receive abundant inhibitory synapses (Wei et al., 2011) and ooDSGC dendrites fail to form stratified arbors when SACs are ablated in neonates (X. Duan and J.R.S., unpublished data). SACs with somata in the inner nuclear and ganglion cell layers interact with the OFF and ON ooDSGC arbors, respectively (Figure 6A). Based on this reasoning, we asked whether Cntn5 ligands are present on ON SAC arbors.

Cntn5 has been shown to bind to PTPRγ and APLP1 (Bouyain and Watkins, 2010; Shimoda et al., 2012). We examined the distribution of these proteins immunohistochemically and found that they were diffusely distributed in the IPL (Figure S6A). In contrast, Cntn5 itself was highly concentrated in S4. It was diffusely distributed through the IPL in neonates but became concentrated in S4 by P6 (Figure 6B). This immunoreactivity could reflect a concentration of Cntn5 on the ON dendrites of ooDGSCs, but an alternative possibility was suggested by further analysis of the *Cntn5*^{LacZ} line, which revealed that ON, but not OFF, SACs express *Cntn5* (Figure 6C). This result suggested that Cntn5 could be localized on SAC dendrites in addition to or instead of ooDSGC dendrites.

To distinguish these possibilities, we used high-resolution confocal microscopy. We triply stained whole mounts of Hb9-GFP retina with antibodies to VAChT and ChAT (to mark SAC dendrites), GFP (to mark ooDSGC dendrites), and Cntn5. Imaging revealed that immunoreactivity was associated with both ON SACs and ON ooDSGC dendrites, whereas little immunoreactivity was present on OFF SACs or OFF ooDSGC dendrites (Figure 6D; Figure S6C). Moreover, the density of Cntn5 puncta in ON ooDSGC dendrites was significantly decreased in *Satb1* mutants (Figure 6E). In contrast, loss of *Satb1* had no effect on expression of *Cntn5* in SACs (Figures S5B and S6B). Thus, ON dendrites of ooDSGCs and dendrites of ON SACs both bear Cntn5, but regulation of their expression differs, being Satb1 dependent in ooDSGCs and Satb1 independent in SACs.

Cntn5 Binds to Caspr4 and Mediates Homophilic Adhesion

If Cntn5 mediates interactions between ooDSGC and SAC dendrites that sculpt the ooDSGC arbor, it must be capable of signaling to the cell interior and binding homophilically. We tested these requirements in turn.

Contactins are attached to the outer leaflet of the plasma membrane by a glycosylphosphatidyl-inositol linkage; they signal to the cell interior through contactin-associated proteins (Casprs), a set of seven transmembrane proteins, with which they form dimers (Poliak and Peles, 2003; Shimoda and Watanabe, 2009). Analysis of our transcriptomic database revealed that all seven Casprs, as well as four other Cntn-binding proteins, were expressed by ooDSGCs, but their expression was not significantly affected by loss of Satb1 (Figure S6D). Because Contactin/Caspr interactions are selective, we performed co-expression and co-clustering assays in heterologous cells to determine which Casprs could dimerize with Cntn5. Cntn1 and Cntn2 associated selectively with Caspr1 and Caspr2, respectively, consistent with previous studies (Figure S6E) (Peles

(F) Mean intensity (±SEM) of GFP-labeled dendritic processes across the IPL from images such as those in (D) (6–8 RGCs per genotype).
(G–K) Dendritic length (G), branch number (H), ON arbor length (I), OFF arbor length (J), and ON/OFF ratio (K) from reconstructed dendrites as shown in (D) (6–8 RGCs per genotype).
See also Figure S5 and Table S1. Scale bars represent 20 μm. ***$p < 0.001$, **$p < 0.01$, *$p < 0.05$ by one-way ANOVA with Bonferroni post-tests.

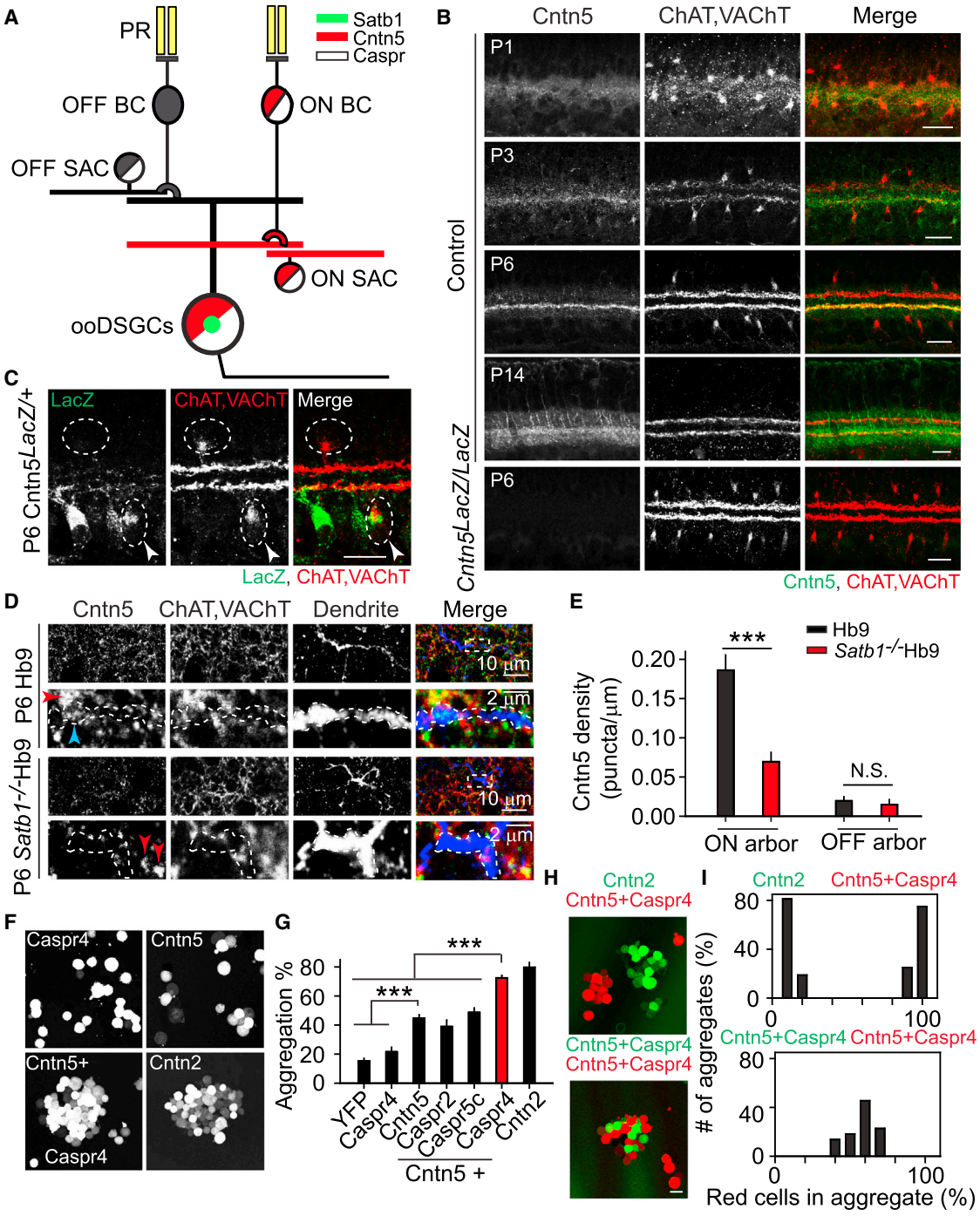

Figure 6. Cntn5 Is Expressed by ON, but Not OFF, SACs and Located in Both ON SAC Plexus and ON Strata of ooDSGC Dendrite

(A) Cells of the direction-selective circuit, indicating expression of Cntn5, Caspr, and Satb1. BC, bipolar cell; PR, photoreceptor.

(B) Anti-Cntn5 (green in merge) and anti-ChAT, VAChT (red in merge) staining from control and *Cntn5*$^{LacZ/\ LacZ}$ retinas at indicated ages.

(C) LacZ staining with SAC markers (ChAT, VAChT) in P6 *Cntn5*$^{LacZ/+}$ retina. SAC somata are outlined by dashed circles. Arrowheads indicate co-labeled cells.

(D) Confocal images of ON retinal strata from P6 Hb9-GFP and *Satb1*$^{-/-}$;Hb9-GFP retinae stained with antibodies to Cntn5 (green), ChAT and VAChT (red), and GFP (blue). Low-power micrographs show stacks; single 0.3 µm planes from boxed regions are shown at higher power below. ooDSGC dendrites in the high-power images are outlined. Red arrowheads indicate Cntn5 puncta colocalized with SAC processes. Blue arrowhead indicates Cntn5 puncta colocalized with ooDSGC dendrite.

(E) Average density (±SEM) of Cntn5 puncta per µm in ooDSGC dendrites. n > 20 for each genotype.

(F) Aggregation of heterologous cells transfected with vectors encoding *Cntns* and/or *Casprs* as indicated.

(legend continued on next page)

et al., 1997; Poliak et al., 2003; Traka et al., 2003). Cntn5 did not associate detectably with Caspr1, Caspr2, Caspr3, or Caspr5c but did co-cluster with Caspr4 (see also Ashrafi et al., 2014), Caspr5a, and Caspr5b. For one of them, Caspr4, we obtained retinas from a reporter line and confirmed that Caspr4 was expressed in both ooDSGCs and SACs as well as several other cell types (Figures S6F and S6G). Thus, appropriate Casprs are present in ooDSGCs to render Cntn5 capable of translating intercellular interactions into intracellular signaling events.

We also used heterologous cells to test whether Cntn5 or Cntn5/Caspr dimers bind homophilically, as previously demonstrated for Cntn2 and Cntn4 (Felsenfeld et al., 1994; Rader et al., 1993; Yamagata and Sanes, 2012). In a previous study (Yamagata and Sanes, 2012), we did not detect homophilic binding of chick Cntn5, but in that study, we did not co-express Casprs with Cntns. We therefore repeated the experiments using mouse Cntns with or without Casprs. Mouse Cntn5 mediated weak aggregation, which was enhanced by co-expression of Caspr4, to a level nearly equivalent to that of Cntn2 (Figures 6F and 6G). Caspr requirements for adhesion mirrored those for dimerization, in that co-expression of Caspr2 or Caspr5c, which do not dimerize with Cntn5, had no effect on aggregation. Adhesion was specific in that Cntn5/Caspr4-expressing cells did not aggregate with Cntn2-expressing cells (Figures 6H and 6I). Together, these results support the idea that homophilic Cntn5/Caspr4 interactions with ON SACs could stabilize ooDSGC ON dendritic arbors.

Conditionally Knocking Down Cntn5 in Either Presynaptic SACs or Postsynaptic ooDGSCs Causes the Similar Loss of ON Arbor

Finally, we designed a direct test of the hypothesis that Cntn5-mediated homophilic interactions stabilize the ON ooDSGC arbor. For this purpose, we used a conditional strategy to attenuate *Cntn5* expression separately in ooDSGCs and SACs. We designed shRNAs against *Cntn5*, assessed their efficacy in heterologous cells (Figures S7A and S7B), and generated an AAV vector to deliver the shRNA in a cre-dependent manner (Yu et al., 2015). We injected the vector intravitreally into either *ChAT*^{Cre};Hb9-GFP mice to attenuate expression in SACs or *vGlut2*^{Cre};Hb9-GFP mice to attenuate expression in ooDSGCs. In both cases, defects in ooDSGCs were indistinguishable from those demonstrated above for the constitutive *Cntn5* mutant: ON arbors were disrupted, OFF arbors persisted, and the decreased length of the ON arbor was equivalent to the increased length of the OFF arbor (Figures 7A–7K; Figures S7C and S7D). The finding that Cntn5 is required in both ON SACs and ooDSGCs to stabilize the ON ooDSGC arbor provides strong evidence that ON SACs provide a scaffold for ooDSGC dendrite maturation and that Cntn5-mediated homophilic binding mediates the intercellular interaction.

DISCUSSION

All RGCs receive inputs from retinal interneurons in the IPL, and their axons send information through the optic nerve to the rest of the brain. Yet, RGCs are a heterogeneous class, with >30 types of RGCs in mice, each tuned to particular visual features (Baden et al., 2016; Sanes and Masland, 2015). Differences among their dendrites are prime determinants of differences in their specific response properties. For example, the size and shape of the dendrite arbor define the approximate size of the receptive field center (Brown et al., 2000; Peichl and Wässle, 1983; Yang and Masland, 1994). Perhaps most striking, dendrites of each RGC type are restricted to specific sublaminae within the IPL. Since afferent processes of amacrine and bipolar interneurons are similarly restricted, the laminar position of an RGC dendrite determines the inputs to which it has access and therefore the visual features to which it responds. Of particular relevance here, OFF RGCs, which respond to decrements in light intensity, have dendrites in the outer part of the IPL, where they receive input from OFF bipolar cells. Conversely, ON RGCs have dendrites in the inner part of the IPL, where they receive input from ON bipolar cells. ooDSGCs respond to both ON and OFF signals because the inner and outer arbors of their bistratified dendrites receive input from ON and OFF bipolars, respectively (Vaney et al., 2012).

Here, we investigated cellular and molecular processes that lead to formation of bistratified ooDSGC dendrites. Initially, ooDSGCs elaborate diffuse arbors in the ON sublaminae of the IPL. Later, they add an OFF arbor and then, over the following few days, restrict both ON and OFF arbors to the narrow strata occupied by SAC dendrites. In the absence of *Satb1*, the OFF arbor forms, but the ON arbor does not. Instead, dendrites in the ON sublaminae grow into the OFF sublaminae (summarized in Figure 3G). Thus, Satb1 is required for the maturation and maintenance of the ON arbor. Satb1 acts in part by regulating the expression (directly or indirectly) of the adhesion molecule Cntn5. Cntn5 in ooDSGCs, in turn, interacts homophilically with Cntn5 in ON SACs, likely as a Cntn5/Caspr4 heterodimer, to anchor ON ooDSGC dendrites. Together, these results reveal a pathway that controls formation of a specific dendritic compartment within a specific RGC type.

Satb1

Satb1 is a homeodomain transcriptional regulator that affects gene expression in two ways: it organizes chromatin globally by anchoring specific DNA sequences to the nuclear matrix, and it affects transcription of specific genes by recruiting chromatin modifiers to their upstream sequences (Galande et al., 2007). Its mechanism of action has been studied most thoroughly in thymocytes (Yokota and Kanakura, 2014), but it has also been implicated in development of several other cell types and in oncogenesis (Brocato and Costa, 2015).

(G) Percentage of cells in aggregates from images such as those in (F). n > 200 cells for each condition.
(H) Cntn5/Caspr4-expressing cells aggregate with each other but segregate from Cntn2-expressing cells. Cells transfected as in (F) were marked with distinct fluorophores to assess co-aggregation.
(I) Percentage of red cells in mixed aggregates from images such as those in (H). n > 200 cells for each condition.
See also Figure S6. Scale bars represent 20 μm in (B, C, F, and H); 10 μm in (D), 2 μm in (D) insets. ***p < 0.001, **p < 0.01, N.S.: p > 0.05, by one-way ANOVA with Bonferroni's post-tests.

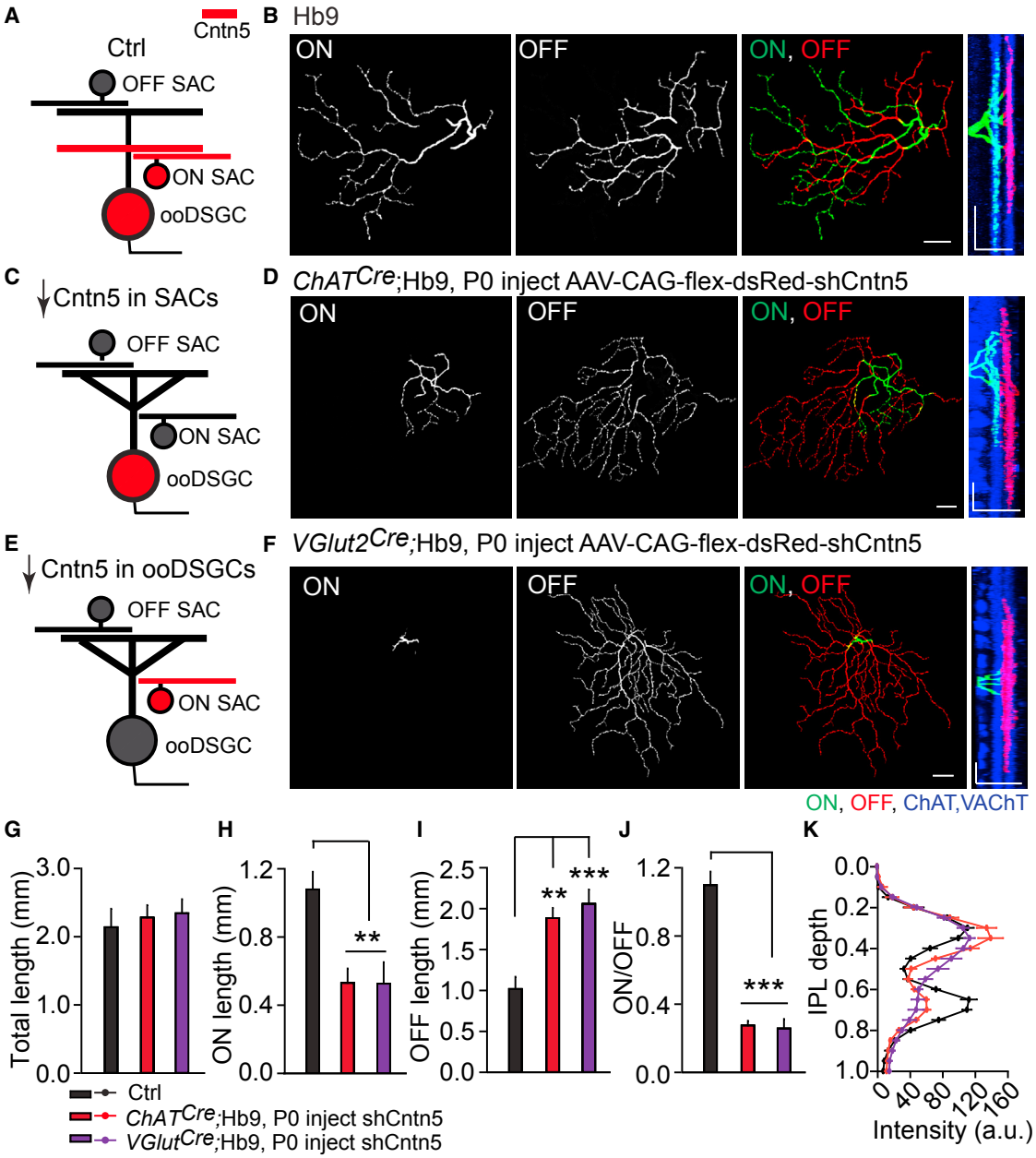

Figure 7. Attenuation of Cntn5 Expression in Either SACs or ooDSGCs Phenocopies Constitutive *Cntn5* Deletion

(A, C, and E) Sketches illustrating experiments shown in (B), (D), and (F). ooDSGCs dendrites are bistratified in controls (A), but monostratified following attenuation of *Cntn5* expression (red) in SACs (using $ChAT^{cre}$) (C) or RGCs (using $Vglut2^{cre}$) (E).

(B, D, and F) Reconstructed dendrites of Hb9-GFP RGCs from P16 retinas of indicated genotypes: Hb9 (B), $ChAT^{cre}$;Hb9 (D), and $vGlut2^{cre}$;Hb9 (F). ON and OFF strata are shown in green and red, respectively. Rotations at right show stratification; S2 and S4 laminae are marked by anti-ChAT and VAChT staining (blue).

(G–J) Dendritic length (G), ON arbor length (H), OFF arbor length (I), and ON/OFF ratio (J) from reconstructed dendrites as shown in (B), (D), and (F) (six RGCs per genotype).

(K) Mean intensity (±SEM) of GFP-labeled dendritic processes across the IPL from images such as those shown in (B), (D), and (F) (six RGCs per genotype). See Figures S7C and S7D for similar results obtained from sectioned retinas.

See also Figure S7. Scale bars represent 20 μm in (B), (D), and (F). ***$p < 0.001$, **$p < 0.01$, by one-way ANOVA with Bonferroni post-tests.

In contrast, few studies have analyzed roles of Satb1 in the nervous system. We show here that Satb1 is required for morphogenesis of ooDSGC dendrites. In its absence, ooDSGCs dendrites become monostratified and lack ON input. The effect of Satb1 is remarkably specific: it has no discernable effect on the generation or survival of ooDSGCs or on their acquisition

of markers that characterize RGCs generally or ooDSGCs specifically. Recently, two groups reported a requirement for Satb1 in terminal differentiation of a population of somatostatin-positive cortical interneurons; in its absence, these interneurons fail to mature and acquire appropriate inputs (Close et al., 2012; Denaxa et al., 2012). Thus, in both retina and cortex, Satb1 affects specific neuronal types and is dispensable for initial differentiation but required for maturation and innervation. In cortex, but not in retina, Satb1 is also required for neuronal migration and survival.

Comparison of two populations of ooDSGCs—V-ooDSGCs and N-ooDSGCs—suggests that Satb2, a homolog of Satb1, may also regulate morphogenesis of ooDSGC arbors. Both genes are expressed in ooDSGCs, although Satb2 is also expressed in other retinal neuronal types (Kay et al., 2011b). Both RGC types lose ON arbors in the absence of Satb1, but the phenotype is less penetrant and more variable in N-ooDSGCs than in V-ooDSGCs. Interestingly, Satb2 appears earlier in N-ooDSGCs than in V-ooDSGCs, and loss of Satb1 is accompanied by downregulation of Satb2 in V-ooDSGCs, but not N-ooDSGCs. Although direct evidence is lacking, these results suggest that the two homologs may cooperate to pattern dendritic arbors.

Contactin 5

The contactins are a family of six immunoglobulin superfamily adhesion molecules. They and their co-receptors—Casprs—are expressed by subsets of neurons throughout the brain and play roles in a variety of developmental processes, ranging from neuronal migration to axon guidance to formation of nodes of Ranvier (Poliak and Peles, 2003; Shimoda and Watanabe, 2009; Zuko et al., 2011). Deletion of the *Cntn5* gene in mice leads to defects in the subcortical auditory pathway and loss of presynaptic inhibitory boutons in spinal cord (Ashrafi et al., 2014; Li et al., 2003; Toyoshima et al., 2009). Polymorphisms in genes encoding several Contactins and Casprs, including *Cntn5*, have been linked to autism (Zuko et al., 2013).

We previously analyzed the expression and roles of three closely related subfamilies of immunoglobulin superfamily molecules in developing chick retina—Contactins, Sidekicks, and Dscams (Goodman et al., 2016; Yamagata and Sanes, 2008; Yamagata et al., 2002). We found that nine of the ten genes in these groups (*Sdk1*, *Sdk2*, *Dscam*, *Dscaml*, and *Cntn1–Cntn5*) were each expressed in discrete, largely non-overlapping subsets of retinal neurons and that processes of neurons that expressed each one were restricted to one or a few sublaminae within the IPL (Yamagata and Sanes, 2012). Using loss- and gain-of-function methods, we showed that at least seven of the proteins (Sdk1, Sdk2, Dscam, Dscaml, and Cntn1–Cntn3) are involved in the patterning of retinal arbors in the IPL. Based on these results, we suggested that these recognition molecules comprise an immunoglobulin superfamily code that regulates dendritic patterning and synaptic specificity in retina. Subsequent genetic analyses in mice have supported this idea for Dscams (Fuerst and Burgess, 2009; Fuerst et al., 2008), Sidekick2 (Krishnaswamy et al., 2015), and, now, Contactin5. The added precision of analysis in mice has shown that these proteins act in somewhat different ways: Dscams by restricting dendrites to appropriate sublaminae, Sdk2 by promoting specific intralaminar connections, and Cntn5 by regulating dendritic morphogenesis.

Contactins are linked to the external surface of the plasma membrane and often signal to the cell interior by forming complexes with transmembrane proteins of the Caspr (contactin-associated protein, also called CNTNAP) family (Shimoda and Watanabe, 2009). We found that Cntn5 can form heterodimers with three of seven Casprs (Caspr4, Caspr5a, and Caspr5b), all of which are expressed by ooDSGCs, and used a reporter line to confirm expression of Caspr4. We did not pursue functional studies of Casprs for three reasons: ooDSGCs express multiple Casprs, they are not detectably regulated by Satb1, and at least Caspr4 is far more broadly distributed than Cntn5.

Contactin 5-Mediated Homophilic Interactions of ooDSGCs Dendrites with SACs

How does Cntn5 act? The most likely idea is that Cntn5 on ooDSGC dendrites interacts with ligands in the inner part of the IPL to stabilize ON dendritic arbors. Although neurites of many cell types contact ooDSGCs during development, we viewed SACs as likely candidates because the ON and OFF ooDSGC arbors fasciculate tightly with the dendrites of ON and OFF SACs, respectively. Moreover, SAC dendrites stratify prior to elaboration of ooDSGC bistratification (Stacy and Wong, 2003), and, in ongoing work, we have found that early postnatal ablation of SACs (using diphtheria toxin) prevents ooDSGC dendrites from forming stratified arbors (X. Duan and J.R.S., unpublished data).

We provide three lines of evidence in support of the idea that the critical interaction between ooDSGCs and ON SACs is mediated by Cntn5/Caspr dimers. First, Cntn5/Casp4 heterodimers mediate homophilic cell-cell interactions. Second, Cntn5 and Caspr4 are both expressed by ON SACs, as well as ooDSGCs, with Cntn5 selectively expressed by ON SACs. This selective expression is highly unusual: ON and OFF SACs are molecularly extremely similar, and to our knowledge, only two proteins have been found that are concentrated in just one type— semaphorin 6A and P2X2 in ON and OFF SACS, respectively (Kaneda et al., 2004; Sun et al., 2013). Third, attenuating expression of *Cntn5* in either ooDSGCs or SACs has the same effect on ooDSGC arbors as global deletion of *Cntn5*.

At this point, we cannot rule out the possibility that other Cntn5-mediated interactions are also involved in patterning ooDSGC dendrites. Cntn5 and Caspr4 are expressed by type 5 bipolar cells, which innervate ON SACs and ON arbors of ooDSGCs (Duan et al., 2014; Shekhar et al., 2016). These bipolar terminals do not form until after ooDSGC arborize, and they are not detectably displaced in *Cntn5* mutants (N.M.T. and J.R.S, unpublished data). Nonetheless, Cntn5-mediated interactions could play a role in stabilizing the axonal arbors of type 5 bipolars, the ON arbors of ooDSGCs, or both. Alternatively, Cntn5 could interact heterophilically with other ligands, although our initial studies of the localization of these proteins do not support the possibility.

In summary, we have characterized some of the molecular circuitry required to endow ooDSGC dendrites with a morphologically striking and functionally critical feature, their dual (ON-OFF) receptivity. Particularly striking is the precision with which Satb1 and Cntn5 sculpt ooDSGC arbors: the ON arbor is deleted (Satb1) or depleted (Cntn5) in their absence, with no apparent

effect on the overall size of the arbor, the magnitude of OFF responses, or direction selectivity. This specificity suggests that a transcriptional hierarchy of at least three levels will be required to explain the morphogenesis of RGC dendrites—a first level that provides RGCs with their identity, a second level that diversifies RGCs into types, and a third level that controls acquisition of sets of specific features. Some members of the first level have been identified (Xiang, 2013), and Satb1 is a member of the third level. Testing this model will require identification of members of the second level.

STAR★METHODS

Detailed methods are provided in the online version of this paper and include the following:

- KEY RESOURCES TABLE
- CONTACT FOR REAGENT AND RESOUCE SHARING
- EXPERIMENTAL MODEL AND SUBJECT DETAILS
  - Mice
- METHOD DETAILS
  - Histology
  - Adeno-Associated Virus
  - Image Acquisition
  - Analysis of Gene Expression
  - Electrophysiology
  - Assays of Cntn/Caspr Interactions
  - Design and Testing of shCntn5 Expression Vectors
- QUANTIFICATION AND STATISTICAL ANALYSIS
- DATA AND SOFTWARE AVAILABILITY

SUPPLEMENTAL INFORMATION

Supplemental Information includes seven figures and one table and can be found with this article online at http://dx.doi.org/10.1016/j.neuron.2017.07.019.

AUTHOR CONTRIBUTIONS

Design of experiments and analysis of data, Y.-R.P., A.K., N.M.T., D.K., and J.R.S.; Histological analysis, Y.-R.P., N.M.T., and E.M.M.; RNA-seq, Y.-R.P.; Cntn/Caspr interactions, A.K., D.K., and Y.-R.P.; Electrophysiology, A.K.; Writing manuscript, Y.-R.P. and J.R.S. with input from other authors.

ACKNOWLEDGMENTS

This work was supported by NIH grants R37NS029169 and R01EY022073 to J.R.S. and a Banting Postdoctoral Fellowship to A.K. We are grateful to Gord Fishell (New York University, NY), Julia Kaltschmidt (Sloan Kettering, NY), Elior Peles (Weizmann Institute, Israel), and Kazutada Watanabe (Nagaoka University) for generously providing mutant mice. We thank Dustin Herrmann and Mallory Laboulaye for assistance.

Received: November 29, 2016
Revised: June 16, 2017
Accepted: July 19, 2017
Published: August 3, 2017

REFERENCES

Ashrafi, S., Betley, J.N., Comer, J.D., Brenner-Morton, S., Bar, V., Shimoda, Y., Watanabe, K., Peles, E., Jessell, T.M., and Kaltschmidt, J.A. (2014). Neuronal Ig/Caspr recognition promotes the formation of axoaxonic synapses in mouse spinal cord. Neuron *81*, 120–129.

Baden, T., Berens, P., Franke, K., Román Rosón, M., Bethge, M., and Euler, T. (2016). The functional diversity of retinal ganglion cells in the mouse. Nature *529*, 345–350.

Bouyain, S., and Watkins, D.J. (2010). The protein tyrosine phosphatases PTPRZ and PTPRG bind to distinct members of the contactin family of neural recognition molecules. Proc. Natl. Acad. Sci. USA *107*, 2443–2448.

Brocato, J., and Costa, M. (2015). SATB1 and 2 in colorectal cancer. Carcinogenesis *36*, 186–191.

Brown, S.P., He, S., and Masland, R.H. (2000). Receptive field microstructure and dendritic geometry of retinal ganglion cells. Neuron *27*, 371–383.

Buffelli, M., Burgess, R.W., Feng, G., Lobe, C.G., Lichtman, J.W., and Sanes, J.R. (2003). Genetic evidence that relative synaptic efficacy biases the outcome of synaptic competition. Nature *424*, 430–434.

Cai, D., Cohen, K.B., Luo, T., Lichtman, J.W., and Sanes, J.R. (2013). Improved tools for the Brainbow toolbox. Nat. Methods *10*, 540–547.

Close, J., Xu, H., De Marco García, N., Batista-Brito, R., Rossignol, E., Rudy, B., and Fishell, G. (2012). Satb1 is an activity-modulated transcription factor required for the terminal differentiation and connectivity of medial ganglionic eminence-derived cortical interneurons. J. Neurosci. *32*, 17690–17705.

Coombs, J., van der List, D., Wang, G.Y., and Chalupa, L.M. (2006). Morphological properties of mouse retinal ganglion cells. Neuroscience *140*, 123–136.

Corty, M.M., Matthews, B.J., and Grueber, W.B. (2009). Molecules and mechanisms of dendrite development in Drosophila. Development *136*, 1049–1061.

Cubelos, B., Sebastián-Serrano, A., Beccari, L., Calcagnotto, M.E., Cisneros, E., Kim, S., Dopazo, A., Alvarez-Dolado, M., Redondo, J.M., Bovolenta, P., et al. (2010). Cux1 and Cux2 regulate dendritic branching, spine morphology, and synapses of the upper layer neurons of the cortex. Neuron *66*, 523–535.

De la Huerta, I., Kim, I.J., Voinescu, P.E., and Sanes, J.R. (2012). Direction-selective retinal ganglion cells arise from molecularly specified multipotential progenitors. Proc. Natl. Acad. Sci. USA *109*, 17663–17668.

Denaxa, M., Kalaitzidou, M., Garefalaki, A., Achimastou, A., Lasrado, R., Maes, T., and Pachnis, V. (2012). Maturation-promoting activity of SATB1 in MGE-derived cortical interneurons. Cell Rep. *2*, 1351–1362.

Dong, X., Shen, K., and Bülow, H.E. (2015). Intrinsic and extrinsic mechanisms of dendritic morphogenesis. Annu. Rev. Physiol. *77*, 271–300.

Duan, X., Krishnaswamy, A., De la Huerta, I., and Sanes, J.R. (2014). Type II cadherins guide assembly of a direction-selective retinal circuit. Cell *158*, 793–807.

Duan, X., Qiao, M., Bei, F., Kim, I.J., He, Z., and Sanes, J.R. (2015). Subtype-specific regeneration of retinal ganglion cells following axotomy: effects of osteopontin and mTOR signaling. Neuron *85*, 1244–1256.

Felsenfeld, D.P., Hynes, M.A., Skoler, K.M., Furley, A.J., and Jessell, T.M. (1994). TAG-1 can mediate homophilic binding, but neurite outgrowth on TAG-1 requires an L1-like molecule and beta 1 integrins. Neuron *12*, 675–690.

Feng, G., Mellor, R.H., Bernstein, M., Keller-Peck, C., Nguyen, Q.T., Wallace, M., Nerbonne, J.M., Lichtman, J.W., and Sanes, J.R. (2000). Imaging neuronal subsets in transgenic mice expressing multiple spectral variants of GFP. Neuron *28*, 41–51.

Fried, S.I., Münch, T.A., and Werblin, F.S. (2002). Mechanisms and circuitry underlying directional selectivity in the retina. Nature *420*, 411–414.

Fuerst, P.G., and Burgess, R.W. (2009). Adhesion molecules in establishing retinal circuitry. Curr. Opin. Neurobiol. *19*, 389–394.

Fuerst, P.G., Koizumi, A., Masland, R.H., and Burgess, R.W. (2008). Neurite arborization and mosaic spacing in the mouse retina require DSCAM. Nature *451*, 470–474.

Furuta, Y., Lagutin, O., Hogan, B.L., and Oliver, G.C. (2000). Retina- and ventral forebrain-specific Cre recombinase activity in transgenic mice. Genesis *26*, 130–132.

Galande, S., Purbey, P.K., Notani, D., and Kumar, P.P. (2007). The third dimension of gene regulation: organization of dynamic chromatin loopscape by SATB1. Curr. Opin. Genet. Dev. *17*, 408–414.

Goodman, K.M., Yamagata, M., Jin, X., Mannepalli, S., Katsamba, P.S., Ahlsén, G., Sergeeva, A.P., Honig, B., Sanes, J.R., and Shapiro, L. (2016). Molecular basis of sidekick-mediated cell-cell adhesion and specificity. eLife *5*, 5.

Grueber, W.B., Jan, L.Y., and Jan, Y.N. (2003). Different levels of the homeodomain protein cut regulate distinct dendrite branching patterns of Drosophila multidendritic neurons. Cell *112*, 805–818.

Hong, Y.K., Kim, I.J., and Sanes, J.R. (2011). Stereotyped axonal arbors of retinal ganglion cell subsets in the mouse superior colliculus. J. Comp. Neurol. *519*, 1691–1711.

Huberman, A.D., Wei, W., Elstrott, J., Stafford, B.K., Feller, M.B., and Barres, B.A. (2009). Genetic identification of an On-Off direction-selective retinal ganglion cell subtype reveals a layer-specific subcortical map of posterior motion. Neuron *62*, 327–334.

Jinushi-Nakao, S., Arvind, R., Amikura, R., Kinameri, E., Liu, A.W., and Moore, A.W. (2007). Knot/Collier and cut control different aspects of dendrite cytoskeleton and synergize to define final arbor shape. Neuron *56*, 963–978.

Kaneda, M., Ishii, K., Morishima, Y., Akagi, T., Yamazaki, Y., Nakanishi, S., and Hashikawa, T. (2004). OFF-cholinergic-pathway-selective localization of P2X2 purinoceptors in the mouse retina. J. Comp. Neurol. *476*, 103–111.

Kay, J.N., De la Huerta, I., Kim, I.J., Zhang, Y., Yamagata, M., Chu, M.W., Meister, M., and Sanes, J.R. (2011a). Retinal ganglion cells with distinct directional preferences differ in molecular identity, structure, and central projections. J. Neurosci. *31*, 7753–7762.

Kay, J.N., Voinescu, P.E., Chu, M.W., and Sanes, J.R. (2011b). Neurod6 expression defines new retinal amacrine cell subtypes and regulates their fate. Nat. Neurosci. *14*, 965–972.

Kay, J.N., Chu, M.W., and Sanes, J.R. (2012). MEGF10 and MEGF11 mediate homotypic interactions required for mosaic spacing of retinal neurons. Nature *483*, 465–469.

Kim, M.D., Jan, L.Y., and Jan, Y.N. (2006). The bHLH-PAS protein Spineless is necessary for the diversification of dendrite morphology of Drosophila dendritic arborization neurons. Genes Dev. *20*, 2806–2819.

Kim, I.J., Zhang, Y., Yamagata, M., Meister, M., and Sanes, J.R. (2008). Molecular identification of a retinal cell type that responds to upward motion. Nature *452*, 478–482.

Kim, I.J., Zhang, Y., Meister, M., and Sanes, J.R. (2010). Laminar restriction of retinal ganglion cell dendrites and axons: subtype-specific developmental patterns revealed with transgenic markers. J. Neurosci. *30*, 1452–1462.

Krishnaswamy, A., Yamagata, M., Duan, X., Hong, Y.K., and Sanes, J.R. (2015). Sidekick 2 directs formation of a retinal circuit that detects differential motion. Nature *524*, 466–470.

Lefebvre, J.L., Sanes, J.R., and Kay, J.N. (2015). Development of dendritic form and function. Annu. Rev. Cell Dev. Biol. *31*, 741–777.

Li, H., Takeda, Y., Niki, H., Ogawa, J., Kobayashi, S., Kai, N., Akasaka, K., Asano, M., Sudo, K., Iwakura, Y., and Watanabe, K. (2003). Aberrant responses to acoustic stimuli in mice deficient for neural recognition molecule NB-2. Eur. J. Neurosci. *17*, 929–936.

Li, W., Wang, F., Menut, L., and Gao, F.B. (2004). BTB/POZ-zinc finger protein abrupt suppresses dendritic branching in a neuronal subtype-specific and dosage-dependent manner. Neuron *43*, 823–834.

London, M., and Häusser, M. (2005). Dendritic computation. Annu. Rev. Neurosci. *28*, 503–532.

Morrie, R.D., and Feller, M.B. (2016). Development of synaptic connectivity in the retinal direction selective circuit. Curr. Opin. Neurobiol. *40*, 45–52.

Osterhout, J.A., Josten, N., Yamada, J., Pan, F., Wu, S.W., Nguyen, P.L., Panagiotakos, G., Inoue, Y.U., Egusa, S.F., Volgyi, B., et al. (2011). Cadherin-6 mediates axon-target matching in a non-image-forming visual circuit. Neuron *71*, 632–639.

Oyster, C.W., and Barlow, H.B. (1967). Direction-selective units in rabbit retina: distribution of preferred directions. Science *155*, 841–842.

Parrish, J.Z., Emoto, K., Kim, M.D., and Jan, Y.N. (2007). Mechanisms that regulate establishment, maintenance, and remodeling of dendritic fields. Annu. Rev. Neurosci. *30*, 399–423.

Peichl, L., and Wässle, H. (1983). The structural correlate of the receptive field centre of alpha ganglion cells in the cat retina. J. Physiol. *341*, 309–324.

Peles, E., Nativ, M., Lustig, M., Grumet, M., Schilling, J., Martinez, R., Plowman, G.D., and Schlessinger, J. (1997). Identification of a novel contactin-associated transmembrane receptor with multiple domains implicated in protein-protein interactions. EMBO J. *16*, 978–988.

Peng, Y.R., He, S., Marie, H., Zeng, S.Y., Ma, J., Tan, Z.J., Lee, S.Y., Malenka, R.C., and Yu, X. (2009). Coordinated changes in dendritic arborization and synaptic strength during neural circuit development. Neuron *61*, 71–84.

Poliak, S., and Peles, E. (2003). The local differentiation of myelinated axons at nodes of Ranvier. Nat. Rev. Neurosci. *4*, 968–980.

Poliak, S., Salomon, D., Elhanany, H., Sabanay, H., Kiernan, B., Pevny, L., Stewart, C.L., Xu, X., Chiu, S.Y., Shrager, P., et al. (2003). Juxtaparanodal clustering of Shaker-like K+ channels in myelinated axons depends on Caspr2 and TAG-1. J. Cell Biol. *162*, 1149–1160.

Puram, S.V., and Bonni, A. (2013). Cell-intrinsic drivers of dendrite morphogenesis. Development *140*, 4657–4671.

Rader, C., Stoeckli, E.T., Ziegler, U., Osterwalder, T., Kunz, B., and Sonderegger, P. (1993). Cell-cell adhesion by homophilic interaction of the neuronal recognition molecule axonin-1. Eur. J. Biochem. *215*, 133–141.

Ramón y Cajal, S. (1909). Histologie du Système Nerveux de L'homme & des Vertébrés (Maloine).

Rieke, F., Lee, A., and Haeseleer, F. (2008). Characterization of Ca2+-binding protein 5 knockout mouse retina. Invest. Ophthalmol. Vis. Sci. *49*, 5126–5135.

Rodriguez, A.R., de Sevilla Müller, L.P., and Brecha, N.C. (2014). The RNA binding protein RBPMS is a selective marker of ganglion cells in the mammalian retina. J. Comp. Neurol. *522*, 1411–1443.

Rossi, J., Balthasar, N., Olson, D., Scott, M., Berglund, E., Lee, C.E., Choi, M.J., Lauzon, D., Lowell, B.B., and Elmquist, J.K. (2011). Melanocortin-4 receptors expressed by cholinergic neurons regulate energy balance and glucose homeostasis. Cell Metab. *13*, 195–204.

Rousso, D.L., Qiao, M., Kagan, R.D., Yamagata, M., Palmiter, R.D., and Sanes, J.R. (2016). Two pairs of ON and OFF retinal ganglion cells are defined by intersectional patterns of transcription factor expression. Cell Rep. *15*, 1930–1944.

Samuel, M.A., Zhang, Y., Meister, M., and Sanes, J.R. (2011). Age-related alterations in neurons of the mouse retina. J. Neurosci. *31*, 16033–16044.

Sanes, J.R., and Masland, R.H. (2015). The types of retinal ganglion cells: current status and implications for neuronal classification. Annu. Rev. Neurosci. *38*, 221–246.

Santiago, C., and Bashaw, G.J. (2014). Transcription factors and effectors that regulate neuronal morphology. Development *141*, 4667–4680.

Shekhar, K., Lapan, S.W., Whitney, I.E., Tran, N.M., Macosko, E.Z., Kowalczyk, M., Adiconis, X., Levin, J.Z., Nemesh, J., Goldman, M., et al. (2016). Comprehensive classification of retinal bipolar neurons by single-cell transcriptomics. Cell *166*, 1308–1323.e30.

Shimoda, Y., and Watanabe, K. (2009). Contactins: emerging key roles in the development and function of the nervous system. Cell Adhes. Migr. *3*, 64–70.

Shimoda, Y., Koseki, F., Itoh, M., Toyoshima, M., and Watanabe, K. (2012). A cis-complex of NB-2/contactin-5 with amyloid precursor-like protein 1 is localized on the presynaptic membrane. Neurosci. Lett. *510*, 148–153.

Stacy, R.C., and Wong, R.O. (2003). Developmental relationship between cholinergic amacrine cell processes and ganglion cell dendrites of the mouse retina. J. Comp. Neurol. *456*, 154–166.

Sugimura, K., Satoh, D., Estes, P., Crews, S., and Uemura, T. (2004). Development of morphological diversity of dendrites in Drosophila by the BTB-zinc finger protein abrupt. Neuron *43*, 809–822.

Sun, L.O., Jiang, Z., Rivlin-Etzion, M., Hand, R., Brady, C.M., Matsuoka, R.L., Yau, K.W., Feller, M.B., and Kolodkin, A.L. (2013). On and off retinal circuit assembly by divergent molecular mechanisms. Science *342*, 1241974.

Toyoshima, M., Sakurai, K., Shimazaki, K., Takeda, Y., Nakamoto, M., Serizawa, S., Shimoda, Y., and Watanabe, K. (2009). Preferential localization of neural cell recognition molecule NB-2 in developing glutamatergic neurons in the rat auditory brainstem. J. Comp. Neurol. *513*, 349–362.

Traka, M., Goutebroze, L., Denisenko, N., Bessa, M., Nifli, A., Havaki, S., Iwakura, Y., Fukamauchi, F., Watanabe, K., Soliven, B., et al. (2003). Association of TAG-1 with Caspr2 is essential for the molecular organization of juxtaparanodal regions of myelinated fibers. J. Cell Biol. *162*, 1161–1172.

Trapnell, C., Roberts, A., Goff, L., Pertea, G., Kim, D., Kelley, D.R., Pimentel, H., Salzberg, S.L., Rinn, J.L., and Pachter, L. (2012). Differential gene and transcript expression analysis of RNA-seq experiments with TopHat and Cufflinks. Nat. Protoc. *7*, 562–578.

Trenholm, S., Johnson, K., Li, X., Smith, R.G., and Awatramani, G.B. (2011). Parallel mechanisms encode direction in the retina. Neuron *71*, 683–694.

Valnegri, P., Puram, S.V., and Bonni, A. (2015). Regulation of dendrite morphogenesis by extrinsic cues. Trends Neurosci. *38*, 439–447.

Vaney, D.I., Sivyer, B., and Taylor, W.R. (2012). Direction selectivity in the retina: symmetry and asymmetry in structure and function. Nat. Rev. Neurosci. *13*, 194–208.

Vong, L., Ye, C., Yang, Z., Choi, B., Chua, S., Jr., and Lowell, B.B. (2011). Leptin action on GABAergic neurons prevents obesity and reduces inhibitory tone to POMC neurons. Neuron *71*, 142–154.

Wei, W., Hamby, A.M., Zhou, K., and Feller, M.B. (2011). Development of asymmetric inhibition underlying direction selectivity in the retina. Nature *469*, 402–406.

Whitney, I.E., Keeley, P.W., St John, A.J., Kautzman, A.G., Kay, J.N., and Reese, B.E. (2014). Sox2 regulates cholinergic amacrine cell positioning and dendritic stratification in the retina. J. Neurosci. *34*, 10109–10121.

Xiang, M. (2013). Intrinsic control of mammalian retinogenesis. Cell. Mol. Life Sci. *70*, 2519–2532.

Yamagata, M., and Sanes, J.R. (2008). Dscam and Sidekick proteins direct lamina-specific synaptic connections in vertebrate retina. Nature *451*, 465–469.

Yamagata, M., and Sanes, J.R. (2012). Expanding the Ig superfamily code for laminar specificity in retina: expression and role of contactins. J. Neurosci. *32*, 14402–14414.

Yamagata, M., Weiner, J.A., and Sanes, J.R. (2002). Sidekicks: synaptic adhesion molecules that promote lamina-specific connectivity in the retina. Cell *110*, 649–660.

Yang, G., and Masland, R.H. (1994). Receptive fields and dendritic structure of directionally selective retinal ganglion cells. J. Neurosci. *14*, 5267–5280.

Yokota, T., and Kanakura, Y. (2014). Role of tissue-specific AT-rich DNA sequence-binding proteins in lymphocyte differentiation. Int. J. Hematol. *100*, 238–245.

Yu, X., Ye, Z., Houston, C.M., Zecharia, A.Y., Ma, Y., Zhang, Z., Uygun, D.S., Parker, S., Vyssotski, A.L., Yustos, R., et al. (2015). Wakefulness is governed by GABA and histamine cotransmission. Neuron *87*, 164–178.

Zuko, A., Bouyain, S., van der Zwaag, B., and Burbach, J.P. (2011). Contactins: structural aspects in relation to developmental functions in brain disease. Adv. Protein Chem. Struct. Biol. *84*, 143–180.

Zuko, A., Kleijer, K.T., Oguro-Ando, A., Kas, M.J., van Daalen, E., van der Zwaag, B., and Burbach, J.P. (2013). Contactins in the neurobiology of autism. Eur. J. Pharmacol. *719*, 63–74.

STAR★METHODS

KEY RESOURCES TABLE

REAGENT or RESOURCE	SOURCE	IDENTIFIER
Antibodies		
Chicken polyclonal anti-GFP	Abcam	CAT#ab13970; RRID: AB_300798
Rabbit polyclonal anti-GFP	Millipore	Cat# AB3080P; RRID: AB_2630379
Rabbit polyclonal anti-Satb1	Abcam	Cat#ab109122; RRID: AB_10862207
Goat polyclonal anti-Satb1	Santa Cruz	CAT#sc-5989; RRID: AB_2184337
Rabbit polyclonal anti-Cart	Phoenix Pharmaceuticals	Cat#H-003-62; RRID: AB_2313614
Rabbit polyclonal anti-mCherry	Cai et al., 2013	N/A
Mouse monoclonal anti-β-galactosidase	DSHB	CAT#40-1a; RRID: AB_2314509
Rabbit polyclonal anti-β-galactosidase	Duan et al., 2014	N/A
Goat polyclonal anti-choline acetyltransferase	Millipore	CAT#AB144P; RRID: AB_11214092
Goat polyclonal Anti-Vesicular Acetylcholine Transporter	Millipore	CAT#ABN100; RRID: AB_2630394
Guinea pig polyclonal anti-Rbpms	PhosphoSolutions	CAT# 1832-RBPMS; RRID: AB_2492226
Rabbit polyclonal anti-Calbindin	Swant	CAT# CB38; RRID: AB_10000340
Mouse monoclonal anti-Calretinin	Millipore	CAT# MAB1568; RRID: AB_94259
Guinea pig polyclonal anti-vGlut3	Chemicon	CAT# AB5421; RRID: AB_2187832
Sheep polyclonal anti-tyrosine hydroxylase	Millipore	CAT# AB1542; RRID: AB1542
Mouse monoclonal anti-Gad65/67	USHB	CAT# Gad-6; RRID: AB_528264
Mouse monoclonal anti-PKCa	Abcam	CAT# ab31; RRID: AB_303507
Rabbit polyclonal anti-Secretagogin	BioVendor	CAT# RD181120100; RRID: AB_2034060
Mouse monoclonal anti-CaBp5	Rieke et al., 2008	N/A
Rat monoclonal anti-Ctip2	Abcam	CAT#ab18465; RRID: AB_2064130
Goat polyclonal anti-Isl1	R&D Systems	Cat# AF1837; RRID: AB_2126324
Mouse monoclonal anti-Brn3a	Millipore	Cat# MAB1585; RRID: AB_94166
Goat polyclonal anti-Brn3b	Santa Cruz	Cat# sc-6026; RRID: AB_673441
Rabbit polyclonal anti-Tbr2	Abcam	Cat# ab23345; RRID: AB_778267
Rabbit polyclonal anti-Melanopsin	Thermo Fisher Scientific	Cat# PA1-780; RRID: AB_2267547
Rabbit polyclonal anti-Foxp2	Abcam	Cat# ab16046; RRID: AB_2107107
Mouse monoclonal anti-Syt2	ZIRC	CAT#Znp-1; RRID: AB_10013783
Rat monoclonal anti-Cntn5	Millipore	CAT#MABN877
Mouse monoclonal anti-Kv4.2	Rockland	Cat# 200-301-G03; RRID: AB_2611209
Rabbit polyclonal anti-Cntn1	Novus	CAT# NBP1-84763; RRID: AB_11026884
Rabbit polyclonal anti-Cntn2	Novus	CAT# NBP1-90054; RRID: AB_11028475
Rabbit polyclonal anti-Cntn5	Novus	CAT# NBP1-83242; RRID: AB_11019867
Rat monoclonal anti-RFP	Chromotek	CAT# 5f8; RRID: AB_2336064
Rabbit polyclonal anti-dsRed	Clontech	Cat# 632496; RRID: AB_10013483
Rat anti-mouse monoclonal CD90.2 (Thy-1.2) PE-Cyanine7	Affymetrix	CAT#25-0902-81; RRID: AB_469641
Rat anti-mouse monoclonal CD90.2 (Thy-1.2) microbeads	MACS Miltenyi Biotec	CAT# 130-049-101
Chemicals, Peptides, and Recombinant Proteins		
Hank's balanced salt solution (HBSS)	Thermo Fisher Scientific	CAT#14170-112
Papain	Worthington	CAT# LS003126
MEM	Invitrogen	CAT#11090099
BSA	Sigma	CAT#A9418-10G
Ovomucoid	Worthington	CAT#LS003087
Large cell column	MACS Miltenyi Biotec	CAT# 130042202

(*Continued on next page*)

Continued

REAGENT or RESOURCE	SOURCE	IDENTIFIER
Superscript III first-strand synthesis super mix for qRT-PCR	Invitrogen	CAT# 11752-050
qPCR SYBR green	Thermo Fisher Scientific	CAT# F410L
Ames Medium	Sigma	A1420-10X1L
Euthasol	Virbac	CAT#710101
Tamoxifen	Sigma	CAT#T5648
Critical Commercial Assays		
Ovation RNA-seq system V2	NuGEN	CAT# 7102-32
Ovation low-input library system	NuGEN	CAT# 0344-32
PicoPure RNA Isolation Kit	Invitrogen	CAT# KIT0204
RNA Clean and Concentrator-5 Kit	Zymo	CAT# R1015
Deposited Data		
Raw data files for RNA sequencing	Gene Expression Omnibus	GEO: GSE90673
Raw data for microarrays	Gene Expression Omnibus	GEO: GSE90673
Experimental Models: Cell Lines		
HEK293 cells	ATCC	N/A
Experimental Models: Organisms/Strains		
Mouse: STOCK Tg(Drd4-EGFP)W18Gsat/Mmnc	MMRRC	000231-UNC; RRID: MMRRC_000231-UNC
Mouse: B6.Cg-Tg(Hlxb9-GFP)1Tmj/J	IMSR	# JAX:005029; RRID: IMSR_JAX:005029
Mouse: TYW3	Kim et al., 2010	N/A
Mouse: TYW7	Kim et al., 2010	N/A
Mouse: STOCK Tg(Cdh3-EGFP)BK102Gsat/Mmnc	MMRRC	#000236-UNC; RRID: MMRRC_000236-UNC
Mouse: Fstl4-CreERT2	Kim et al., 2010	N/A
Mouse: STOCK Tg(Jam2-cre/ERT2)2Jrs/J	Kim et al., 2008	Stock No: 029417; RRID: IMSR_JAX:029417
Mouse: B6.129(SJL)-*Kcng4*$^{tm1.1(cre)Jrs}$/J	Duan et al., 2014	Stock No: 029414; RRID: IMSR_JAX:029414
Mouse: B6.Cg-Tg(Thy1-EYFP)15Jrs/J	Feng et al., 2000	Stock No: 005630; RRID: IMSR_JAX:005630
Mouse: B6.Cg-Tg(Thy1-YFP)HJrs/J	Feng et al., 2000	Stock No: 003782; RRID: IMSR_JAX:003782
Mouse: Satb1floxed C57BL/6N-*Satb1*$^{tm1a(EUCOMM)Hmgu}$/J	Close et al., 2012	N/A
Mouse: STOCK Tg(Six3-cre)69Frty/GcoJ	The Jackson Laboratory	Stock No: 019755; RRID: IMSR_JAX:019755
Mouse: STOCK Tg(Cartpt-cre)1Aibs/J	The Jackson Laboratory	Stock No: 009615; RRID: IMSR_JAX:009615
Mouse: Cntn5^{tm1Kwat}/Cntn5^{tm1Kwat}	Li et al., 2003	RRID: MGI_3051993
Mouse: *Caspr4*^{GFP}	Ashrafi et al., 2014	N/A
Mouse: Vglut2-ires-Cre	IMSR	RRID: IMSR_JAX:016963
Bacterial and Virus Strains		
AAV9.CAG.Flex.tdTomato.WPRE.bGH (AllenInstitute864) (titer: 1e12)	Penn Vector Core	CAT# AV-1-ALL864
AAV2/9-CAG-Cre	Boston Children's Hospital	N/A
AAV2/9-CAG-Flex-dsRed-shCntn5-2	Boston Children's Hospital	N/A
Oligonucleotides		
Primer: Cntn5 (primer set 1) Forward GGAAAGATACCGAGCCAGAAG	IDT	N/A
Primer: Cntn5 (primer set 1) Reverse GACTGTGAGGTGATAGAGTGTG	IDT	N/A
Primer: Cntn5 (primer set 2) Forward CTGCTGCCATTTTGAAGAGTGT	IDT	N/A
Primer: Cntn5 (primer set 2) Reverse TGAGTCTCCAACAGGAAGCCAT	IDT	N/A
Primer: Cntn5 (primer set 3) Forward ACTCCTCAGATGCCTTCAGACA	IDT	N/A

(*Continued on next page*)

Continued

REAGENT or RESOURCE	SOURCE	IDENTIFIER
Primer: Cntn5 (primer set 3) Reverse AGTTCCATTCCGAAGCCATCTG	IDT	N/A
Primer: GAPDH Forward GTGGAGTCATACTGGAAC ATGTAG	IDT	N/A
Primer: GAPDH Reverse AATGGTGAAGGTCGGTGTG	IDT	N/A
shCntn5-1 target sequence: AGTGTTTGGCTGAGAATAAAT	IDT	N/A
shCntn5-2 target sequence: GCAGATTTAATGATCAGGAAC	IDT	N/A
shCntn5-3 target sequence: GCAGACAGTGTGTCAGATGAG	IDT	N/A
shCntn5-4 target sequence: CTGGATGATGCCGGAATATAC	IDT	N/A
Software and Algorithms		
Tophat2	Trapnell et al., 2012	RRID: SCR_013035
Cufflinks	Trapnell et al., 2012	http://cole-trapnell-lab.github.io/cufflinks/; RRID: SCR_014597
Cuffdiff	Trapnell et al., 2012	http://cole-trapnell-lab.github.io/cufflinks/; RRID: SCR_001647
IGV	Broad Institute	https://www.broadinstitute.org/igv/; RRID: SCR_011793
ImageJ	NIH	http://rsb.info.nih.gov.ezp-prod1.hul.harvard.edu/ij/index.html; RRID: SCR_003070
Pairwise stitching ImageJ plugin	NIH	http://imagej.net/Image_Stitching
Segmentation Simple Neurite Tracer ImageJ plugin	NIH	http://imagej.net/Simple_Neurite_Tracer
AnalyzeSkeleton ImageJ plugin	Ignacio Arganda-Carreras	http://imagej.net/AnalyzeSkeleton
Interactive Stack Rotation ImageJ plugin	Stephan Saafeld	http://imagej.net/Interactive_Stack_Rotation
Zen	Zeiss	RRID: SCR_013672; https://www.zeiss.com/microscopy/en_us/products/microscope-software/zen.html
FluoView FV1000	Olympus	N/A
GraphPad Prism	GraphPad	RRID: SCR_002798
Other		
Agilent BioAnalyzer 2100	Agilent	N/A
Illumina Nestseq 500	Illumina	N/A

CONTACT FOR REAGENT AND RESOUCE SHARING

Further information and requests for reagents may be directed and will be fulfilled by the Lead Contact and corresponding author Joshua R. Sanes (sanesj@mcb.harvard.edu).

EXPERIMENTAL MODEL AND SUBJECT DETAILS

Mice

All animal experiments were approved by the Institutional Animal Care and Use Committees (IACUC) at Harvard University. Mice were maintained in a pathogen-free facility under standard housing conditions with continuous access to food and water. The RNaseq experiments were carried out at postnatal age (P) 6. Histological studies used P1-21 mice unless indicated otherwise. Electrophysiological analysis was performed on adults (2-3 months). Both male and female mice were used in all studies in roughly equal numbers. We noted no sexual dimorphisms in any results reported here. None of the mice had noticeable health or immune status abnormalities, and were not subject to prior procedures. The genotype of mice is described where appropriate.

The following mouse lines were used:

1. *Satb1* conditional allele (*Satb1*^{fl}) (C57BL/6N-*Satb1*$^{tm1a(EUCOMM)Hmgu}$/J) was a gift from G. Fishell (Close et al., 2012). To generate a constitutive mutant, the floxed segment was deleted in the germline using *Cre.*
2. *Six3-Cre* mice express *Cre* in most of the retina, excluding the far periphery (Furuta et al., 2000).
3. Hb9-GFP transgenic mice express GFP in ooDSGCs that prefer ventral motion (Trenholm et al., 2011). This expression reflects a position effect; *Hb9* is not expressed endogenously in these cells.
4. DRD4-GFP BAC transgenic mice express GFP in ooDSGCs that prefer nasal motion (Huberman et al., 2009; Kay et al., 2011b). This expression reflects a position effect; *Drd4* is not expressed endogenously in these cells.
5. FSTL4-CreER mice, express CreER in ooDSGCs that prefer ventral motion (Kim et al., 2010). This expression reflects a position effect; *Fstl4* is not expressed endogenously in these cells.
6. Thy1-stop-YFP Lines #1 and #15 transgenic mice express YFP in a cre-dependent manner in many neuronal population (Buffelli et al., 2003).
7. JamB-CreER BAC transgenic mice express CreER in a population of RGCs called J-RGCs that prefer ventral motion at the offset of illumination (Kim et al., 2008).
8. Kcng4$^{tm1.1(cre)Jrs}$ mice express *Cre* in Type 5 bipolar cells and alpha RGCs (Duan et al., 2014, 2015).
9. Cdh3-GFP BAC transgenic mouse express GFP in several sets of RGCs including bistratified intrinsically photosensitive RGCs (Osterhout et al., 2011).
10. Thy1-YFP-H transgenic mice express YFP in approximately 200 RGCs per retina (Feng et al., 2000; Samuel et al., 2011).
11. TYW3 transgenic mice express YFP in several sets of monostratified RGCs that laminate in S3 (Kim et al., 2010; Krishnaswamy et al., 2015).
12. TYW7 transgenic mice express YFP in two sets of monostratified OFF alpha (Kim et al., 2010).
13. *Cntn5*^{lacZ} "knock-in" mice express tau-lacZ from the endogenous *Cntn5* locus (*Cntn5*^{tm1Kwat}), generating a null allele of *Cntn5* (Li et al., 2003).
14. *Caspr4*^{GFP} "knock-in" mice express GFP from the endogenous *Caspr4* locus (Ashrafi et al., 2014).
15. *ChAT*^{Cre} mice express Cre in cholinergic neurons without disrupting endogenous ChAT expression (Rossi et al., 2011).
16. *vGlut2*^{Cre} mice express Cre in excitatory glutamatergic neurons without disrupting endogenous VGluT2 expression (Vong et al., 2011).

METHOD DETAILS

Histology

Mice were euthanized with intraperitoneal injection of euthasol (Virbac), and either enucleated immediately or transcardially perfused with Ringer's solution followed by 4% paraformaldehyde (PFA) in PBS. Eye cups were removed and fixed in 4% PFA on ice for 1 hr. Retinas were then dissected, post-fixed for an additional 30 min and then rinsed with PBS and analyzed as whole mounts or after sectioning in a cryostat (Leica) as described by (Duan et al., 2014; Kim et al., 2010).

Antibodies used were as follows: chick and rabbit anti-GFP (1:500, Abcam; 1:5000, Millipore); rabbit and goat anti-Satb1(1:1000, Epitomics; 1:500, Santa Cruz); rabbit anti-Cart (1:2000, Phoenix Pharmaceuticals); rabbit anti-mCherry (1:1000, homemade); rabbit and mouse anti-β-galactosidase (1:5000, homemade; 1:1000, DSHB); goat anti-choline acetyltransferase (1:500, Millipore); goat anti-VAChT (1:1000, Millipore); guinea pig anti-Rbpms (1:5000, PhosphoSolutions); rabbit anti-Calbindin (1:2000, Swant); mouse anti-Calretinin (1:5000, Millipore); guinea pig anti-VGLUT3 (1:2500, Millipore); sheep anti-tyrosine hydroxylase (TH) (1:2000, Millipore); mouse anti-Gad65/67 (1:1000, Millipore); mouse anti-PKCa (1:1000, Abcam); rabbit anti-Secretagogin (1:10,000; BioVendor); mouse anti-CaBP5 (1:50, gift from Dr. Francoise Haeseleer); rat anti-Ctip2 (1:500, Abcam); goat anti-Isl1 (1:1000, R&D systems); mouse anti-Brn3a (1:500, Millipore); goat anti-Brn3b (1:1000, Santa Cruz); rabbit anti-Tbr2 (1:1000, Abcam); rabbit anti-Melanopsin (1:5000, Thermo scientific); rabbit anti-Foxp2 (1:1500, Abcam); mouse anti-Kv4.2 (1:1000, Rockland); and rabbit anti-dsRed (1:1000, Clontech). Nuclei were labeled with DAPI (1:1000, Invitrogen). Secondary antibodies were conjugated to Alexa Fluor 488, 568, and 647 (Invitrogen) and used at 1:1000. Fluoromount-G (SouthernBiotech) was used for mounting wholemounts. ProLong Gold Antifade was used for mounting retina section slides.

Brains from perfused animals were post-fixed in 4% PFA at 4°C overnight, and then sunk in 30% sucrose, embedded in Tissue Freezing Medium (EMS) and cryosectioned at 50 μm thickness. Brain sections were stained with chicken anti-GFP (1:500) for 5 days 4°C, them counterstained with DAPI, mounted and imaged.

Adeno-Associated Virus

Intravitreal injection of AAV was performed as previously described (Hong et al., 2011). P 0-3 pups were anesthetized on ice for 5 min and AAV virus was introduced with a fine glass pipette using a Picospritzer (Parker) to control pressure. Four AAV vectors were used: AAV2-CAG-flex-tdTomato (University of Pennsylvania AAV core), AAV2-CAG-LSL-YFP (University of Pennsylvania

AAV core), AAV2-CAG-Cre (Childrens Hospital Boston AAV core), and AAV2-CAG-flex-dsRed-shCntn5 (Childrens Hospital Boston AAV core). Infection sites were visualized by anti-tdTomato, anti-GFP, or anti-dsRed staining.

Image Acquisition

Images were acquired on Olympus FV1000 MPE or Zeiss LSM 710 confocal microscopes with 405, 488-515, 568, and 647 lasers, processed using Zeiss ZEN or Olympus Fluoview FV1000 software suites, and analyzed using ImageJ (NIH). Section images were acquired with a 40X oil lens at the resolution of 1024X1024 pixels, a step size of 0.8 μm, and 90 μm pinhole size. Images for dendritic reconstruction were scanned at a step size of 0.2-0.3 μm, 40 μm pinhole size. Images of whole retinas were acquired with a 20X oil lens at a resolution of 1024X1024 pixels, a step size of 1.0 μm, and 90 μm pinhole size. Images for anti-Cntn5 staining in whole mounts were scanned at a step size of 0.3 μm, 40 μm pinhole size.

Analysis of Gene Expression

We used the microarray datasets described in (Kay et al., 2011b, 2012), supplemented with new arrays from Hb9-GFP and Drd4-GFP RGCs and horizontal cells. Briefly, retinal neurons expressing fluorescent proteins were purified by fluorescence-activated cell sorting (FACS), and amplified cDNA was hybridized with Affymetrix microarrays. Data were analyzed using GeWorkbench software. The gene expression level from individual samples was normalized to the total expression level of the gene across all the samples and transformed into log2 value.

For RNaseq, Hb9-GFP cells from wild-type or *Satb1*$^{-/-}$ retina were FACS sorted at P6. Five replicates for each genotype. Libraries were generated using the Ovation RNA-Seq and Ultralow System V2 kits (Nugen). Libraries were sequenced with Illumina NextSeq High 75 cycle, single-end reads.

For RT-PCR, total RNA was isolated and purified from FACS sorted cells using a PicoPure RNA Isolation Kit (Invitrogen). DNase treatment was performed to remove genomic DNA using RNA Clean & Concentrator- 5 Kit (Zymo). First strand cDNA synthesis was done using the Superscript III reagents (Invitrogen). RT-PCR was carried out using DyNAmo HS SYBR green qPCR kits (Thermo). ddCt values were used to detect Cntn5 levels with the expression of GAPDH as internal control. Three primer sets for Cntn5 are: 1) GGAAAGATACCGAGCCAGAAG (Forward), and GACTGTGAGGTGATAGAGTGTG (Reverse); 2) CTGCTGCCATTTTGAAGAGTGT (Forward), and GACTGTGAGGTGATAGAGTGTG (Reverse); 3) ACTCCTCAGATGCCTTCAGACA (Forward), and AGTTCCATTCC GAAGCCATCTG (Reverse). GAPDH primer set: GTGGAGTCATACTGGAAC ATGTAG (Forward), and AATGGTGAAGGTCGGTGTG (Reverse).

Electrophysiology

Electrophysiological analysis was performed as described previously (Krishnaswamy et al., 2015). Briefly, mice were dark-adapted for > 2 hr and retinas were dissected in oxygenated (95% O2; 5% CO2) Ames solution heated to ~30-32°C. Relaxing cuts were made and the retina was placed in a recording chamber with ganglion cells facing upward and the dorsal-quadrant of the retina marked for orientation. GFP cells were then visualized under a two-photon microscope and targeted for loose patch recording using patch electrodes (3-5MΩ) filled with Ames medium. Monochrome stimuli (410nm) were presented by a projector controlled by the psychophysics toolbox in MATLAB. Receptive field centers were determined with small flashing spots, and then stimulated by presenting a long bar moving along its long axis in 8 different directions to test for direction selectivity. Direction selective index was computed as previously (Duan et al., 2014).

Assays of Cntn/Caspr Interactions

cDNAs encoding all annoted Cntns and Casprs in the mouse genome were cloned from a mouse brain cDNA library and the products were cloned into pCR8-TOPO (Life Technologies). Cntns and Casprs were then subcloned into modified expression vectors using Gateway cloning: pCAGS-RfA for Contactins and pUb-mCherry for Casprs (creating Caspr-mCherry fusion proteins).

To assay cis-interactions of Cntns with Casprs, human embryonic kidney (HEK) 293 cells obtained from ATCC were cultured on poly-L-lysine coated coverslips and co-transfected with expression vectors using TransIT-2020 (Mirus). To cluster Cntns/Casprs on the surface of HEK cells, living cell cultures were rinsed with PBS, incubated with rabbit anti-contactin antibodies (1:200 in HEPES-buffered Opti-MEM Reduced Serum Medium) for 30 min at room temperature, rinsed with PBS, fixed with 4% paraformaldehyde/PBS for 1 min, and methanol-treated at −20°C for 15 min. Coverslips were then stained with rat anti-RFP antibody, rinsed with PBS, and stained with secondary antibodies. Coverslips were inverted, mounted on glass slides using Fluoromount-G, and imaged after drying. Positive clustering was defined as the detection of colocalization of two antibodies.

We also assayed Cntn/Caspr-mediated cell-cell interactions in HEK293T cells. However, because these cells endogenously express N-cadherin, which results in substantial endogenous adhesion, we used a line in which expression of N-cadherin was fully eliminated by disrupting both alleles of the N-cadherin gene using CRISPR-mediated gene disruption. HEK293-Ncad-negative cells were co-transfected with Cntn and Caspr vectors described above, along with a cDNA expressing a fluorescent protein, using TransIT-X2 Dynamic Delivery System (Mirus). Aggregation was then assayed as described by (Yamagata and Sanes, 2008). Two days after transfection, the cells were dissociated with 0.05% trypsin in the presence of EDTA for 20 min at 37°C. The reaction was stopped by egg

white trypsin inhibitor. Cells were then divided into 24 well culture dishes in PBS (Ca^{2+} Mg^{2+} free) supplemented with 1% BSA, 20mM HEPES and 1μg/ml DNase I, and rotated at 84 rpm at 37°C for 45 min-1 hr. Aggregation% was defined as 1- [all the parts (after aggregation)/total cells].

Design and Testing of shCntn5 Expression Vectors

The strategy for designing shCntn5 in cre-dependent AAV vector was adapted from Yu et al. (2015). Briefly, hairpin (sh) oligonucleotides were designed online (http://katahdin.mssm.edu/siRNA/RNAi.cgi?type=shRNA). The shCntn5 sequences tested were:

shCntn5-1: GCTGTTGACAGTGAGCGAAGTGTTTGGCTGAGAATAAATTAGTGAAGCC
ACAGATGTAATTTATTCTCAGCCAAACACTGTGCCTACTGCCTCGGA
shCntn5-2:TGCTGTTGACAGTGAGCGCGCAGATTTAATGATCAGGAACTAGTGAA
GCCACAGATGTAGTTCCTGATCATTAAATCTGCATGCCTACTGCCTCG
shCntn5-3:TGCTGTTGACAGTGAGCGCGCAGACAGTGTGTCAGATGAGTAGTG
AAGCCACAGATGTACTCATCTGACACACTGTCTGCTTGCCTACTGCCTCGGA
shCntn5-4:TGCTGTTGACAGTGAGCGCCTGGATGATGCCGGAATATACTAGTGA
CCACAGATGTAGTATATTCCGGCATCATCCAGTTGCCTACTGCCTCGGA

The oligunucleotides were amplified and cloned into pPRIME-dsRed vector. The knockdown efficiency by individual shCntn5 was assessed in HEK293 cells and the shRNA with the highest efficacy, shCntn5-2, was subcloned into AAV-CAG-flex vector.

QUANTIFICATION AND STATISTICAL ANALYSIS

ImageJ (NIH) software was used to generate maximum intensity projections. Plots of intensity across the IPL were processed as following: max projected section images were straightened using the straighten function in ImageJ, based on VAChT/ChAT-positive dendritic bands within the IPL. The whole IPL depth was outlined with ON and OFF SAC somata labeling the inner and outer limit, and divided into 20 bins ranging from 0 (outer)-1(inner). Fluorescence intensities from individual bins were normalized to the total intensity for each image.

For reconstruction of dendrites from whole mounts, well-isolated GFP-positive cells were chosen from sparsely labeled regions, usually in the periphery. Dendrites were manually traced with the simple neurite tracer from ImageJ. Traced cells were filled out by volume and transformed to Z for the stratification analysis as described above. Dendritic length and branch number were calculated using skeleton analysis and multipoint tools in ImageJ.

GFP cell numbers from a 1X1 mm square region were counted at 3-4 locations per retina. X-Y cell coordinates, marked manually, were used to calculate DRP statistics and the distance of exclusive radius as described by Kay et al. (2012).

Hb9 dendritic branches from either ON or OFF arbor were isolated to quantify Cntn5 puncta density. Both the dendritic length and number of Cntn5 puncta located in the dendrite were measured. The density of Cntn5 puncta were calculated as number of Cntn5 puncta per μm of Hb9 dendrite.

RNaseq data were analyzed using Tuxedo tools (Trapnell et al., 2012). Briefly, sequenced reads were mapped to the mouse genome (mm10) via Tophat, transcripts were counted via Cufflinks, and differentially expressed genes were detected with Cuffdiff or t test.

All data are shown as Mean ± SEM with n representing the cell number from at least three mice or independent experimental replicates. Statistical analyses were performed using Graphpad prism 6. Two-tailed Student's t tests were used for two group comparisons, and one-way ANOVA followed by Bonferroni's post-tests were used for multiple comparisons. Statistical details can be found in Figures and Figure Legends.

DATA AND SOFTWARE AVAILABILITY

The accession number for the raw and processed microarray and RNA-seq data reported in this paper is GEO: GSE90673.